Magnetism and deformation of epitaxial Pd and Rh thin films

Tomáš Káňa,[1,2] Erwin Hüger,[3] Dominik Legut,[4] Miroslav Čák,[5] and Mojmír Šob[6,2,7,*]

[1]*Central European Institute of Technology, CEITEC IPM, Institute of Physics of Materials, Academy of Sciences of the Czech Republic, Žižkova 22, CZ-616 62 Brno, Czech Republic*

[2]*Institute of Physics of Materials, Academy of Sciences of the Czech Republic, Žižkova 22, CZ-616 62 Brno, Czech Republic*

[3]*Clausthal University of Technology, Institute of Metallurgy, Microkinetics Group, D-38678 Clausthal-Zellerfeld, Germany*

[4]*IT4Innovations Center, VŠB-Technical University of Ostrava, 17. listopadu 15, CZ-708 33 Ostrava, Czech Republic*

[5]*Interdisciplinary Center for Advanced Materials Simulation, Ruhr-Universität Bochum, Universitätstrasse 150, D-44780 Bochum, Germany*

[6]*Central European Institute of Technology, CEITEC MU, Masaryk University, Kamenice 5, CZ-625 00 Brno, Czech Republic*

[7]*Department of Chemistry, Faculty of Science, Masaryk University, Kotlářská 2, CZ-611 37 Brno, Czech Republic*

(Received 5 January 2016; revised manuscript received 18 March 2016; published 19 April 2016)

By means of *ab initio* calculations, we investigated structural and magnetic properties of Pd and Rh thin films, determining their lattice parameters and epitaxial stresses when they are grown on various substrates, and provided a comparison with available experimental data. Further, we studied in detail the magnetic properties of Pd in the higher-energy hcp structure and of Rh in the higher-energy bcc structure. The results predict that the hcp(11$\bar{2}$0) Pd films [grown by epitaxy on the Nb(001) substrate] should not be ferromagnetically ordered. Concerning the hcp Pd, we mainly investigated the influence of the hcp c/a ratio on the hcp film stability and on the ferromagnetic order. It turns out that the c/a ratio has to be below 1.622 to induce the ferromagnetic order in hcp Pd. We proposed a technological route for obtaining ferromagnetic hcp(11$\bar{2}$0) Pd films and explained the experimentally observed ferromagnetism in twinned Pd nanoparticles induced by strain. We also found that bcc Rh is ferromagnetically ordered, but it cannot be stabilized in the form of thin films. Therefore, we investigated the dependence of ferromagnetic order in bct Rh on the tetragonal c/a ratio and compared our results with experiments performed on Rh/Fe(001) multilayers.

DOI: 10.1103/PhysRevB.93.134422

I. INTRODUCTION

Given a system of point particles in classical mechanics, one can estimate the equilibrium state using the principle of virtual work [1]. Similarly, given a quantum mechanical system of atoms arranged in a periodical lattice, one can estimate its equilibrium volume by letting the volume change and choosing that one minimizing the total energy of the system. The situation becomes much more interesting if the system is subject to some constraints.

An example is a thin film that grows on a substrate. If epitaxial growth occurs, then at least one of the crystallographic directions of the film is parallel with the corresponding crystallographic direction of the substrate (see Fig. 1).

Further, if the film grows pseudomorphically with the substrate, then the lateral periodicity of the film is the same as that of the substrate. As a result, both in-plane lattice parameters of the film are constrained.

Allowing the interlayer distance to relax and minimizing the total energy of the system with the constraints, we can determine the equilibrium structure of the layers of a thin film on a substrate. The film may be still regarded as a bulk material (periodically repeated in all directions), but the constraints on the structural parameters enforce the desired pseudomorphic (or only epitaxial) relationship with the substrate.

The constraints due to the epitaxial relationship of the film and substrate enforce epitaxial stress in the heterostructure. From the theoretical point of view, one can calculate how big the stress is and hence assess the structure stability of the film. Further, the stability of crystalline modifications of thin films and their new physical properties can be theoretically predicted.

Many of the results of modern applied physics have been obtained just by the research on thin films. A general example is a decades-long research on the epitaxial growth of semiconductor heterostructures that has provided the base of modern electronic devices used today.

From the theoretical point of view, much of the experimental work can be made more efficient if experimentalists can exploit the theoretical prediction of *ab initio* calculations. Recent examples of such predictions include ferroelectricity in TiO_2 (Ref. [2]), electrocaloric effect in $BaTiO_3$ (Ref. [3]), or insulator-metal transition in $LaTiO_3$ (Ref. [4]).

This study is focused on palladium and rhodium and their magnetic properties. Not only do their outer atoms on the surface perform catalytic work [5,6] and help to dissociate molecules in the vicinity of the surface, but the film itself may gain new structural or magnetic properties if grown on a suitable substrate [7–13] or in a form of multilayers [14]. Here we do not have in mind the enhancement of magnetic moments of atoms close to the surface or a grain boundary [15] but a complete altering of magnetic behavior (e.g., from paramagnetic to ferromagnetic) of the whole film [9,16–18].

It is noteworthy to point out that searching for magnetic properties of normally nonmagnetic materials in the form of epitaxial heterostructures applies not only to metals but, for example, to Ga(Mn)As semiconductors [19].

Some of the experimental works that have attracted our interest to study theoretically the 4*d* metals Pd and Rh are (i) the growth of hcp Pd(11$\bar{2}$0) films on Nb(001) [8,12,13] and on W(001) substrates [9,11] and (ii) the growth of bct Rh in Fe/Rh

*mojmir@drs.ipm.cz

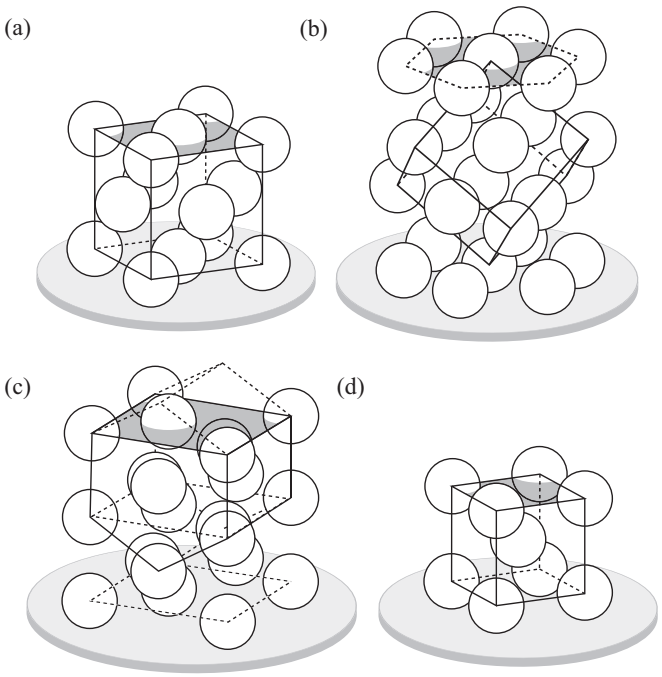

FIG. 1. Considered orientations of fcc and hcp Pd films and fcc and bcc Rh films with respect to the substrate. The substrates have the (a) fcc(001), (b) fcc(111), (c) hcp(11$\bar{2}$0), and (d) bcc(001) orientation.

multilayers [14]. The question is if a normally paramagnetic metal such as Pd and Rh in the form of thin films can exhibit ferromagnetic properties if grown in different crystalline modification and/or be strained due to epitaxial misfit with the substrate. At last, a study of possible ferromagnetic ordering in these 4*d* metals is a logical continuation of the study of the thin films of ferromagnetic 3*d* metals Fe, Co, and Ni [20–23].

As an additional product of this research, new technological routes may be found. For example, recent experimental works show that ferromagnetism in fcc twinned Pd nanoparticles can be induced by strain [24]. This indicates a possibility to use the altered Pd structure as a very sensitive strain gauge. This is possible if one notes that the *ABAB* stacking of the (0001) atomic planes in hcp Pd film can be, in principle, regarded as a perturbed *ABC* fcc stacking with a vast number of inserted stacking faults. Moreover, a thin film is, in principle, more suitable to handle, technologically, than a nanoparticle. Further, calculations in Ref. [25] provide a very low energy difference between paramagnetic and ferromagnetic hcp Pd, of the order of meV/atom. This indicates a very low Curie temperature of the hcp Pd phase and could be greatly exploited in magneto-optical devices where laser power is increased to heat the material to the Curie point in a single spot.

Other calculations that may have technological impact concern ferromagnetism in Pd films that can be driven by applying an electric field [26]. Also, calculations [27–29] have predicted ferromagnetism in Pd thin films induced by quantum wells. These findings have been experimentally confirmed by later experiments with thin Pd films grown on $SrTiO_3$(100) substrate [30].

Calculations on Rh have predicted that Rh thin films grown on Ag(001) substrate may be ferromagnetic up to two monolayers [31,32]. Similarly, calculations for a Rh monolayer grown on Cu(001) substrate and capped with one Cu monolayer [33] found the Rh monolayer to be ferromagnetic, though with a small value of magnetic moment of 0.057 μ_B/atom. All these findings may have a technological impact.

When making theoretical examination of a thin film one needs to know the present stress and strain. For this purpose, a curve depicting the variation of the total energy with the nearest-neighbor distance D_{NN} in the plane of the film parallel to the substrate was calculated and, using its numerical derivative, the variation of epitaxial stress in the film σ^{epi} with D_{NN} was obtained [21–23]. It turned out that the use of the bulk model under constraints set by the substrate was in many cases surprisingly accurate in determining the structure parameters of the film, demonstrating also a strong predicting power: For example, the experimentally determined structure parameters of Fe overlayers grown on the Ir(001) substrate [34] agreed remarkably well with the theoretical prediction obtained with the help of a previously calculated total-energy contour plot for bulk iron presented in Ref. [20].

The behavior of σ^{epi} calculated for a set of given structures with variable D_{NN} can be confirmed by additional points determined by experimentalists. They can choose a particular substrate with a given nearest-neighbor distance D_{NN} and measure the interlayer distance d of the film grown on it. Interestingly enough, *ab initio* calculations can predict just those regions of D_{NN} that correspond to a strained film with physically interesting properties.

Another example is the study of strained tetragonal states of V, Co, and Cu [35], V, Ti, and Sr [36], and V, Nb, Ru, La, Os, and Ir [37], as well as of tetragonal and trigonal states in Po [38,39]. On the whole, the search for regions with unusual physical properties is the main goal of this study.

In the present work, we investigate several crystalline structures of Pd and Rh thin films which can be grown on various substrates (Fig. 1). We determine their lattice parameters and in-plane stresses. More light is shed on the discussion of possible ferromagnetic ordering in hcp Pd [9,25,40,41], where we have found a region of existence of ferromagnetism (FM) depending on the atomic volume and c/a ratio of lattice constants. Similarly, we have investigated the ferromagnetic ordering of bcc Rh discussed in Refs. [17,18,31] and [42].

The paper is organized as follows. After introducing and describing the methods of calculations in Sec. II, Sec. III presents the results regarding the structure and epitaxial stresses in Pd and Rh films for different orientations with respect to the substrate. These results are thoroughly discussed in Sec. IV. Concluding Sec. V summarizes the whole work. A considerable number of figures necessary for discussion of the theoretical predictions are referred throughout the text in Secs. III and IV.

II. METHODS OF CALCULATION

The deformation of the bulk structure consists of lowering its symmetry by stretching the corresponding film along directions parallel to the substrate. For example, the bulk fcc structure illustrated in Fig. 1(a) can be stretched along the

[100] and [010] directions or, respectively, along the [110] and [1$\bar{1}$0] directions.

Apart from the in-plane nearest-neighbor distance D_{NN} mentioned in the previous section, we also introduce the interlayer distance d, similarly as in Ref. [21]. For both the fcc(001) and the fcc(111) planes we have $D_{\mathrm{NN}} = a_{\mathrm{fcc}}/\sqrt{2}$, where a_{fcc} is the lattice constant of the fcc structure.

On the other hand, the epitaxial relationship of an hcp(11$\bar{2}$0) film on bcc(001) substrate [Fig. 1(c)] is different. For example, the first two layers of Pd film grow pseudomorphically with the bcc W(001) substrate [7,11] or with the Nb(001) substrate [8,13]. On top of these two layers, islands of hcp Pd film appear. For the islands $D_{\mathrm{NN}} = c_{\mathrm{hcp}}/2$.

For the bcc structure [Fig. 1(d)], D_{NN} has the same value as the lattice constant of the bcc structure a_{bcc}.

The interlayer distance d for undeformed structures is $a_{\mathrm{fcc}}/2$ [Fig. 1(a)], $a_{\mathrm{fcc}}\sqrt{3}/3$ [Fig. 1(b)], $a_{\mathrm{hcp}}/2$ [Fig. 1(c)], and $a_{\mathrm{bcc}}/2$ [Fig. 1(d)].

Following the ideas presented in Ref. [21], we calculate a curve that exhibits the variation of total energy of the elementary unit cell E with the in-plane distance D_{NN}. For situations illustrated in Figs. 1(a) and 1(d), it is straightforward to determine the epitaxial stress σ^{epi} in the film. Let ϵ denote the in-plane strain of the film,

$$\epsilon = \frac{a}{a_0} - 1, \tag{1}$$

where a_0 and a represent the in-plane lattice constant before and after the strain is applied. Further, let A denote the area of that face of the elementary unit cell that is perpendicular to the direction of a and a_0. The employed unit cell is tetragonal. It may either have the ratio of lattice parameters c/a close to the value of $\sqrt{2}$ and thus represent the face-centered tetragonal structure [close to the fcc structure, Fig. 1(a)], or it can exhibit c/a close to the value of 1 and represent the body-centered tetragonal structure [close to bcc structure, Fig. 1(d)]. In both cases

$$A = ac. \tag{2}$$

The σ^{epi} in the film is then calculated via the numerical derivative of E with respect to the strain as

$$\sigma^{\mathrm{epi}} = \frac{1}{2}\frac{1}{Aa_0}\frac{\partial E}{\partial \epsilon}. \tag{3}$$

For each value of ϵ in Eq. (3) we perform the relaxation of the tetragonal lattice constant c that is perpendicular to the substrate. Equation (3) applies also for calculation of epitaxial stress in the fcc(111) films [Fig. 1(b)]. There the fcc(111) structure of the film is described within a hexagonal unit cell that contains three hexagonal layers ABC and has the lattice parameters $a_{\mathrm{hex}} = a_{\mathrm{fcc}}/\sqrt{2}$ and $c_{\mathrm{hex}} = a_{\mathrm{fcc}}\sqrt{3}$. When applying the strain ϵ, it is more convenient to switch to an orthorhombic unit cell with lattice parameters $a_{\mathrm{hex}}\sqrt{3}$, a_{hex}, and c_{hex}. The area A of that face of the orthorhombic unit cell that is perpendicular to the direction of a_{hex} is

$$A = a_{\mathrm{hex}}\sqrt{3}\,c_{\mathrm{hex}}. \tag{4}$$

Equations (1) and (3) hold in the same form noting that the lattice parameters a and c now stand for a_{hex} and c_{hex}.

The situation is quite different for the epitaxial relationship illustrated in Fig. 1(c). Here, the hcp(0001) atomic planes are perpendicular to the surface of the substrate and two constraints apply in the plane of the substrate surface: one for $D_{\mathrm{NN}} = c_{\mathrm{hcp}}/2$ and the other for a_{hcp} [11,43]. In order to determine the epitaxial stress in those hcp(11$\bar{2}$0) Pd films, we have approximated it by an uniaxial stress σ^{uni} along the [0001] direction. With ϵ being the strain of the hexagonal unit cell in the [0001] direction,

$$\epsilon = \frac{c}{c_0} - 1, \tag{5}$$

and A the area of the (0001) face of the hexagonal lattice,

$$A = a^2\frac{\sqrt{3}}{2}, \tag{6}$$

the uniaxial stress is computed as

$$\sigma^{\mathrm{uni}} = \frac{1}{Ac_0}\frac{\partial E}{\partial \epsilon}. \tag{7}$$

For each value of ϵ in Eq. (7) we perform the Poisson contraction of the area A that is perpendicular to the direction of c and c_0.

The total energy E is calculated using the full-potential linearized augmented plane wave method (FLAPW) as implemented in the WIEN2k code [44]. For exchange-correlation energy, we used the local (spin) density approximation LDA [45]. It is a common wisdom that LDA gives a good description of the 4d metals. Further justification of using LDA for calculating the electronic structure of Pd is that it gives the correct nonmagnetic ground state of fcc Pd. In Fig. 2(a) we can see that the ferromagnetic energy gain $E_{\mathrm{NM}} - E_{\mathrm{FM}}$ is much less than the estimated error of the calculations (0.8 meV/atom) in the whole range of atomic volumes studied. This is not so if other available approximations of exchange-correlation energy are used. Namely, the PBE [46], PBE-sol [47], and Wu-Cohen [48] approximations yield an incorrect ferromagnetic ground state of fcc Pd. The ferromagnetic energy gain given by PBE at the equilibrium volume is very small (2 meV/atom) and for PBE-sol and Wu-Cohen xc energy it is almost negligible. However, calculations in those approximations retain a nonzero magnetic moment for fcc Pd [Figs. 2(b)–2(d)]. This is in contradiction with experimental findings.

There is one disadvantage of using LDA for electronic structure calculations of Pd and Rh and this is the underestimation of equilibrium atomic volume by 3.69% (Pd) and 3.55% (Rh) and overestimation of the bulk modulus by 18% (Pd) and 19% (Rh) (see Tables I and II). To overcome this difficulty, we introduced a *volume correction* that causes the value of equilibrium volume to be equal to the experimental value (Figs. 3 and 4). When performing the volume correction, the shape of the cell is kept and only its volume is multiplied by $(\frac{a_{\mathrm{exp}}}{a_{\mathrm{eq}}})^3$ where a_{exp} and a_{eq} are the experimental and equilibrium lattice constants of fcc Pd and Rh, respectively. Multiplying all the lattice constants with the same number increases the equilibrium volume of the (tetragonal or hexagonal) unit cell so that it is now equal to the experimental value. It means that the zero stress is found at the experimental atomic volume

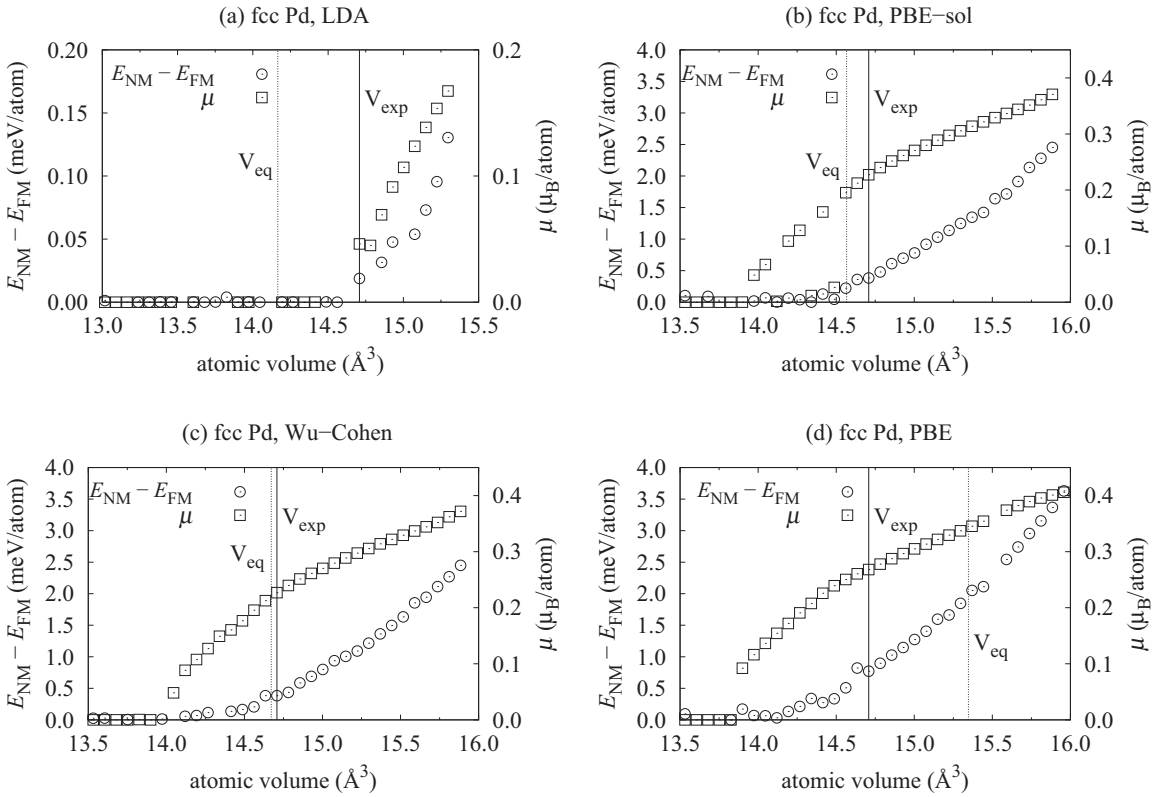

FIG. 2. Variation of the ferromagnetic energy gain $E_{NM} - E_{FM}$ and magnetic moment μ per atom for fcc Pd and various exchange-correlation energy functionals. The Wu-Cohen functional (c) gives the best agreement of the Pd lattice constant with experiment. Note a different energy scaling in panel (a).

(Figs. 5–7, 14, and 15). The lattice parameters a and c of the tetragonal (or hexagonal) unit cell remain in the same proportion as they were before the volume correction was applied. It also means that the shape of the unit cell keeps being fixed. The effect of applying volume correction to the calculated values of σ^{epi} and σ^{uni} in Eqs. (3) and (7) is very small: They are lowered by about 3%–4% with respect to the uncorrected case.

The effect of the volume correction may be seen in plots of energy volume curves of fcc Pd (Fig. 3) and fcc Rh (Fig. 4). The main reason for introducing the volume correction is to reproduce the equilibrium lattice parameters of the Pd and Rh films as well as possible. Together with the fcc ground states of Pd and Rh we have considered the higher-energy states of hcp Pd and bcc Rh as those structures are promising candidates for ferromagnetic ordering. It is seen that at higher volumes of hcp Pd and bcc Rh the ferromagnetic (FM) ordering is energetically favored with respect to both nonmagnetic (NM) and antiferromagnetic (AFM) ordering. [The AFM ordering in hcp Pd and bcc Rh has been considered as if the Pd atoms in subsequent (0001) hcp atomic planes and Rh atoms in subsequent (001) bcc atomic planes had antiparallel alignment of their magnetic moments.] The energetics of the FM and AFM orderings in hcp Pd and bcc Rh is shown in Figs. 12 and 18 in the next sections. Further, if not stated otherwise, the volume correction is applied in all illustrations.

The details of calculations of the total energy are as follows. We have kept the radii of muffin-tin spheres constant at 2.34 a.u. for Pd and at 2.30 a.u. for Rh. The energy dividing the valence and (semi)core electrons has been set to −7.0 Ry and the product of muffin-tin radius and the maximum reciprocal space vector, $R_{MT}K_{max}$, was equal to 8.8. The maximum value ℓ for the waves inside the atomic spheres, ℓ_{max}, was set to 10 and the magnitude of the largest reciprocal vector G in the charge Fourier expansion, G_{max}, was equal to 16. We employed 20 000 k-points in the first Brillouin zone in the mesh generated by the Monkhorst-Pack scheme [53] for the fcc structure and

TABLE I. Calculated and experimental lattice constants and elastic moduli of fcc Pd.

	Lattice constant (Å)	B (GPa)	c_{11} (GPa)	c_{12} (GPa)	c_{44} (GPa)
Experiment [49]	3.8893	195	234	176	71
This work (LDA)	3.8409	230	277	207	82
Reference [50] (LDA)	3.8624	201			

TABLE II. Calculated and experimental lattice constants and elastic moduli of fcc Rh.

	Lattice constant (Å)	B (GPa)	c_{11} (GPa)	c_{12} (GPa)	c_{44} (GPa)
Experiment [51]	3.8034	269	422	192	194
This work (LDA)	3.7578	320	499	231	218
Reference [50] (LDA)	3.7763	312			
Reference [52] (LDA)	3.77	309	482	222	206

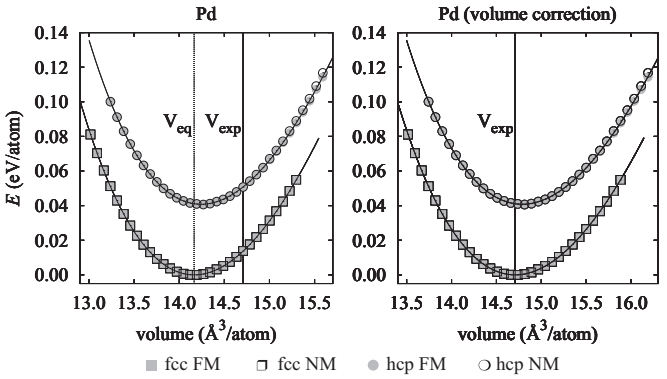

FIG. 3. (Left) The energy-volume curves for fcc and hcp Pd. Vertical lines denote the experimental and equilibrium atomic volumes. (Right) The same after the *volume correction*.

used a similar density of k-points for all other structures. The energy convergence criterion was 2×10^{-5} eV/atom and, on the basis of the convergence tests with respect to the number of k-points and $R_{\mathrm{MT}}K_{\max}$, the error in calculated total energies may be estimated to be less than 8×10^{-4} eV/atom.

III. RESULTS

A. Palladium

The dependence of total energy on D_{NN} mentioned in the previous section has been computed for fcc Pd films grown on the (001) substrates [Figs. 1(a) and 1(d)] and on the (111) substrates [Fig. 1(b)]. The calculated structural parameters of a Pd film grown on the (001) substrate and the corresponding epitaxial stresses present in such a film are shown in Fig. 5. The available experimental data corresponding to Fe(001), Au(001), MgO(001), and $SrTiO_3$(001) substrates have been taken from Refs. [54–56] and [30]. These experimental data indicate that the growth of the Pd film at the MgO substrate is only epitaxial and not pseudomorphic. The data for the $SrTiO_3$, Fe, and Au substrates indicate pseudomorphic growth of the Pd(001) film.

Generally, the experimental interlayer distance d varies with the thickness of the measured film. Assuming the bulk model of the film, the points represent those experimental values of d that were measured in the thickest films and the error bars show the variance of d and D_{NN} measured in Pd(001) films with different thicknesses.

However, the bulk model need not always be the best one. An example is the Pd(001) film grown on the MgO(001) substrate [56] (see Fig. 5). It exhibits larger lattice mismatch: $(a_{\mathrm{Pd}}-a_{\mathrm{MgO}})/a_{\mathrm{MgO}}=-7.64\%$. If coherent Pd islands are grown on MgO(001) with a coverage of less than 0.2 monolayers, then the interlayer distance $d=1.895$ Å is close to the bulk value 1.945 Å. However, a 12.5-monolayer-thick Pd film grows in the form of incoherent islands with disordered dislocations and its interlayer distance decreases to 1.785 Å.

We have further predicted the lattice parameters of pseudomorphic body-centered tetragonal Pd films as they have been experimentally grown on the Nb(001) [8,13], W(001) [7,11], and V(001) [57] substrates (see Table III and Fig. 5).

The noise in epitaxial stress close to the value of $D_{\mathrm{NN}}=2.87$ Å is not attributed to ferromagnetism. It is only a noise in the calculations of the total energy.

Figure 6 shows the dependencies of epitaxial stresses and lattice constants of Pd(111) films grown on various fcc(111), hcp(0001), and bcc(110) substrates. The available experimental data for Pd(111) films have been found in Refs. [58] and [59] for Ni(111) and in Refs. [40,60–69] for Cu(111), Ru(0001), Re(0001), FeO(111), Pt(111), Al_2O_3(0001), $Al_2O_3(2\bar{1}\bar{1}0)$, and W(110) substrates.

The value of interlayer distance d for Pd film grown on Ni(111) substrate has been estimated roughly as a step height of a terrace using scanning tunneling microscope [59]. Other values of interlayer distances have been determined using more sophisticated methods, such as low-energy electron diffraction (LEED) or reflection high-energy electron diffraction (RHEED). Our lattice parameters of Pd films grown on Ru(0001), $Al_2O_3(2\bar{1}\bar{1}0)$, and W(110) substrates agree very well with experimental data (see Fig. 6). It indicates that these three substrates are very suitable for pseudomorphic growth of the Pd(111) film. Concerning fcc(111) Pd films on the other substrates, the experimental values of their in-plane distance D_{NN} and interlayer distance d deviate from the theoretical line in Fig. 6. This, on the contrary, indicates only epitaxial growth of the fcc(111) Pd films on those substrates, but not pseudomorphic growth.

The hcp$(11\bar{2}0)$ Pd film is depicted in Fig. 1(c). First, at this epitaxial relationship, the axis of the hexagonal honeycomb is positioned parallel to the substrate surface and the atoms in $(11\bar{2}0)$ Pd planes form a zigzag pattern [43]. The hcp$(11\bar{2}0)$ Pd layers grow epitaxially on Nb(001) and W(001) substrates [7,8,11–13]. Depending on the in-plane lattice constant of the substrate, there is a good fit in one of the [0001] and $[1\bar{1}00]$ directions, while in the other direction the fit is not so good. It results in island growth where the islands have a shape of elongated orthogonal rectangular domains that are mutually interlocked. The hcp crystalline phase in the films is stabilized inside these domains. The network of domain boundaries inhibits dislocation motion and thus a phase transition back to the ground-state fcc structure of Pd [43].

In an attempt to simplify the situation, we have modeled only uniaxial deformation in the [0001] direction (i.e., in the direction of c_{hcp}) and relaxed the lattice parameters in the directions perpendicular to [0001]. Figure 7 shows that

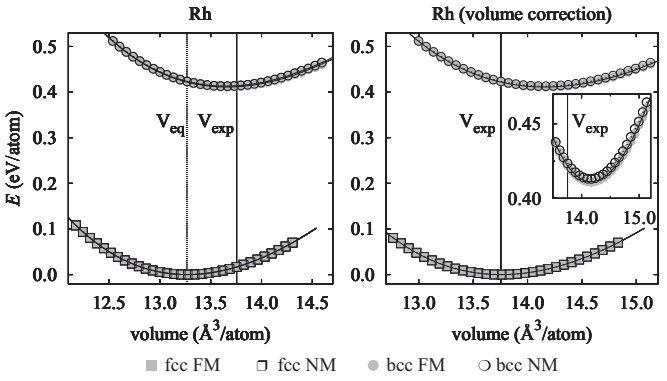

FIG. 4. (Left) The energy-volume curves for fcc and bcc Rh. Vertical lines denote the experimental and equilibrium atomic volumes. (Right) The same after the *volume correction*.

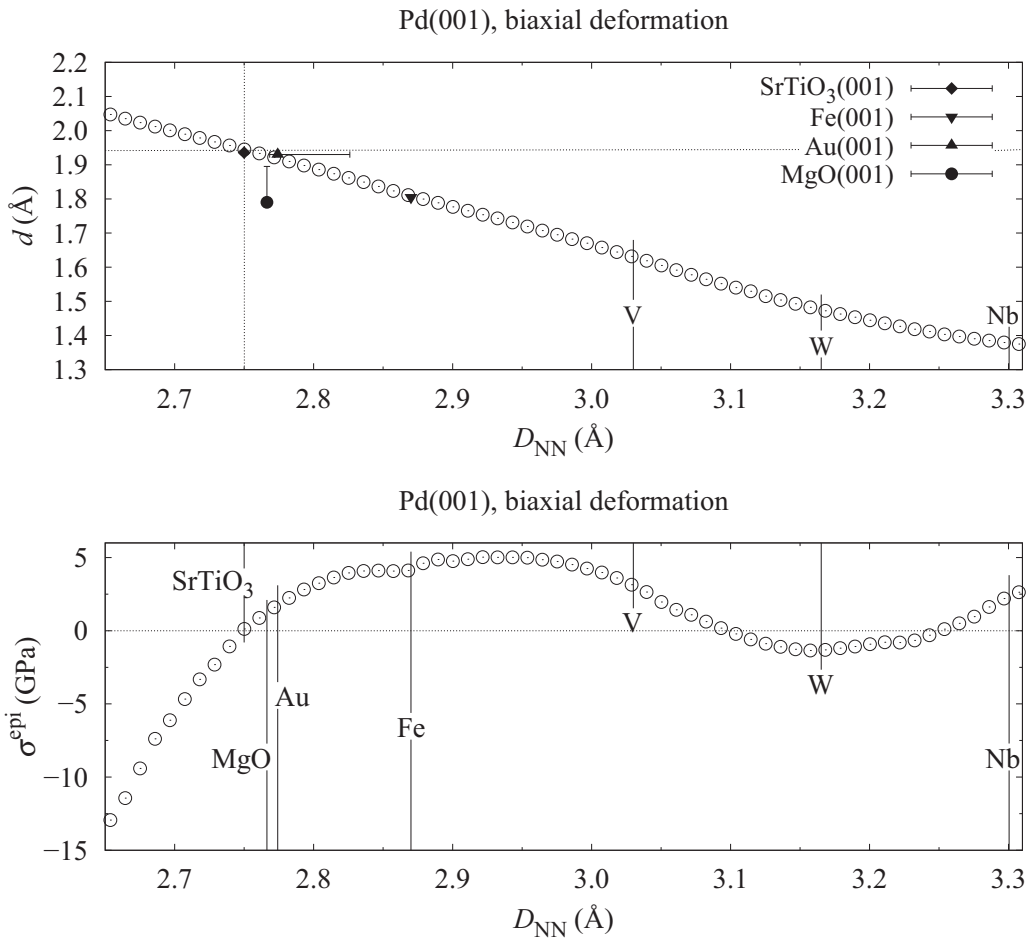

FIG. 5. The interlayer distances d (top) and epitaxial stresses σ^{epi} (bottom) of Pd films grown on (001) substrates as functions of the nearest-neighbor distance D_{NN} in the plane of the film. The dotted lines denote the values of d and D_{NN} for experimentally determined fcc structure of Pd (top) and zero epitaxial stress (bottom). The error bars show the variance of d and D_{NN} measured in the Pd(001) films with various thicknesses.

this treatment can be justified for hcp(11$\bar{2}$0) Pd films grown on bcc(001) substrates. The experimental value of interlayer distance d is now available only for the Nb(001) substrate [70].

Similarly as in Refs. [20,22,23] and [36], we have illustrated both biaxial and uniaxial deformation of Pd and its total energy per atom E in the coordinates of c/a and V/V_{exp}. The results are contour plots of energy as a function of two variables: (1) c/a is the ratio of lattice parameters of elementary unit cell and (2) V/V_{exp} is the relative atomic volume with respect to the experimental atomic volume. The unit cell can be tetragonal for Pd films on fcc(001) substrates or hexagonal for Pd films grown on fcc(111) or hcp(0001) substrates. The body-centered tetragonal structure that corresponds to the fcc structure of Pd has $a_{tetra} = a_{fcc}/\sqrt{2}$ and $c_{tetra} = a_{fcc}$; therefore, $c_{tetra}/a_{tetra} = \sqrt{2}$ (Fig. 8).

If the fcc structure is specified in terms of a hexagonal unit cell [Fig. 1(b)], then $a_{hex} = a_{fcc}/\sqrt{2}$ and $c_{hex} = a_{fcc}\sqrt{3}$ (fcc body diagonal). As a result, $c_{hex}/a_{hex} = \sqrt{6}$ (Fig. 9).

The last considered system is the structure of hcp(11$\bar{2}$0) Pd film growing on bcc(001) substrates. In the calculations, it is described in terms of a hexagonal unit cell with the relaxed ratio of $c_{hcp}/a_{hcp} = 1.68$ (see Fig. 10). This equilibrium value is similar to the experimentally observed value of 1.67 (Refs. [43,70]). The jump on the biaxial deformation path at $c/a = 1.51$ in Fig. 10 is due to a change of magnetic moment from more than 0.3 μ_B/atom to zero as is shown in Fig. 11.

Together with these contour plots of total energy we also present the biaxial and uniaxial deformation paths. In Fig. 8 they correspond to epitaxial and uniaxial Bain paths discussed in Refs. [20,22] and [35].

It may bee seen in Figs. 8 and 9 that the uniaxial and biaxial deformation paths intersect at the points of high symmetry, as are, for example, the points of $c/a = \sqrt{2}$ and $V/V_{exp} = 1$ of the fcc structure and the point of $c/a = 1$ and $V/V_{exp} = 1.01$ corresponding to the bcc structure (Fig. 8).

TABLE III. The predicted lattice parameters a_{bct} and c_{bct} of pseudomorphic bct Pd films grown on bcc substrates. The value a_{bct} is the same as the bcc lattice constant of the corresponding substrate; the value of c_{bct} equals $2d$ (see Fig. 5).

Substrate	a_{bct} (Å)	c_{bct} (Å)
Nb(001)	3.300	2.756
W(001)	3.165	2.950
V(001)	3.030	3.261

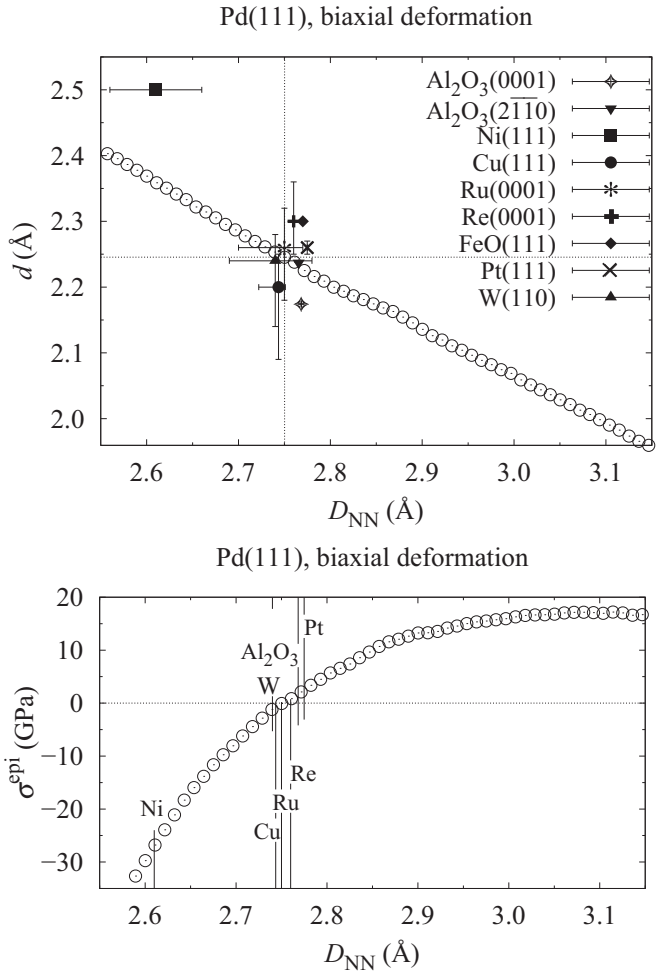

FIG. 6. The interlayer distances d (top) and epitaxial stresses σ^{epi} (bottom) of Pd films grown on the fcc(111), hcp(0001), hcp($2\bar{1}\bar{1}0$), and bcc(110) substrates as functions of the nearest-neighbor distance D_{NN} in the plane of the film. The dotted lines denote the values of d and D_{NN} for experimentally determined fcc structure of Pd (top) and zero epitaxial stress (bottom). The error bars show the variance of d and D_{NN} measured in the Pd(111) films with various thicknesses.

In an attempt to search for possible ferromagnetic ordering in altered Pd structures, we have studied the behavior of atomic magnetic moment per unit cell with respect to atomic volume (Fig. 12). The ratio of c_{hcp}/a_{hcp} was relaxed for every volume considered. Also, Fig. 13 exhibits the DOS of hcp Pd for various uniaxial deformations.

B. Rhodium

Analogously to Pd, we determined the lattice parameters of Rh(001) and Rh(111) films and their epitaxial stresses (Figs. 14–18). The connection between our results for Rh(001) films and the experimental findings about Fe/Rh multilayers [14] is given in Sec. IV. The results for Rh(111) films presented in Figs. 15 and 17 agree with experiment [71] that reports a pseudomorphic growth of a three monolayers thick Rh film on the Ru(0001) substrate. Photoelectron diffraction study of Rh nanoparticles grown on Fe_3O_4/Pd(111) ultrathin film [72] has shown that the first interlayer distance $d_{Rh1\text{-}Rh2}$ is 2.072 Å, while the next interlayer distances $d_{Rh2\text{-}Rh3}$ and $d_{Rh3\text{-}Rh4}$ amount to the bulk value of 2.195 Å.

Again, as in the case of Pd, we have considered both biaxial and uniaxial deformation of Rh and its total energy per atom E in the coordinates of c/a and V/V_{exp}.

We have studied the behavior of atomic magnetic moment per unit cell with respect to atomic volume. In agreement with Refs. [10,18] and [73] we have found one candidate for ferromagnetic ordering: bcc Rh (Fig. 18). This promising finding is, however, somewhat obscured by the fact that the bcc structure is not the ground-state structure of Rh and any technological route for producing magnetic Rh films must first solve the task of stabilizing bcc Rh films. Generally, our research adds bcc Rh to the group of bulklike tetragonal films with ferromagnetic order. The calculated ferromagnetic ordering in bcc Rh has been probably overlooked in the systematic study of the stabilization of such films given in Ref. [74].

IV. DISCUSSION

A comparison of Figs. 14 and 15 to Figs. 5 and 6 illustrates that it is much more difficult to deform Rh than Pd. The difference in epitaxial stresses is very well seen in the case of Pd(001) and Rh(001) films where the maximum of σ^{epi} in Rh (30.8 GPa) exceeds six times the maximum of σ^{epi} in Pd (5.1 GPa). A similar difference is found between Rh(111) and Pd(111) films where the maximum of σ^{epi} amounts to 37.4 and 17.4 GPa, respectively. The hcp($11\bar{2}0$) Pd films exhibit somewhat higher maximum uniaxial stresses (−22.4 GPa in compression and 28.3 GPa in tension) in the [0001] direction than the biaxial stresses in Pd(001) and Pd(111) films. These values are comparable to the values of maximum uniaxial stresses in the [111] direction of fcc(111) Pd films (not shown in Figs. 5–7, 14, and 15). Those are −31.8 GPa in compression and 28.7 GPa in tension. Unlike tensile stresses, the compressive stresses of fcc Pd in the [111] direction and of hcp Pd in the corresponding [0001] direction differ. Hcp Pd is by about 30% more compliant to compression than fcc Pd.

This can be exploited technologically, as the compressed hcp Pd is a good candidate for a ferromagnetic Pd film. The open squares in Figs. 10 and 11 represent the uniaxial deformation path of the hcp($11\bar{2}0$) film in the [0001] direction. (The biaxial deformation path of hcp Pd corresponding to circles was added only for a better comparison with Fig. 9.) It is obvious that hcp Pd films with a lower ratio c/a are more prone to become ferromagnetically ordered. The maximum compressive stress of hcp Pd is found at about $D_{NN} = c_{hcp}/2 = 1.92$ Å (Fig. 7). This corresponds to the value of $d = a_{hcp}/2 = 1.50$ Å and thus the maximum attainable ratio of c/a is 1.28. This is far below the range of c/a between 1.513 and 1.622, where ferromagnetism is most likely to occur (see the plateau where magnetic moment amounts to 0.3 μ_B in Fig. 11).

To obtain a ferromagnetic hcp Pd film at a lowered c/a ratio, one needs to compress the hcp($11\bar{2}0$) Pd structure in the [0001] direction. In such a way one can reach the ferromagnetic region exhibited in Fig. 11. The uniaxial deformation path passes through the ferromagnetic region. As an example, there is one square symbol belonging to that path that has the hexagonal ratio $c/a = 1.564$. It is by about 7% lower than the calculated

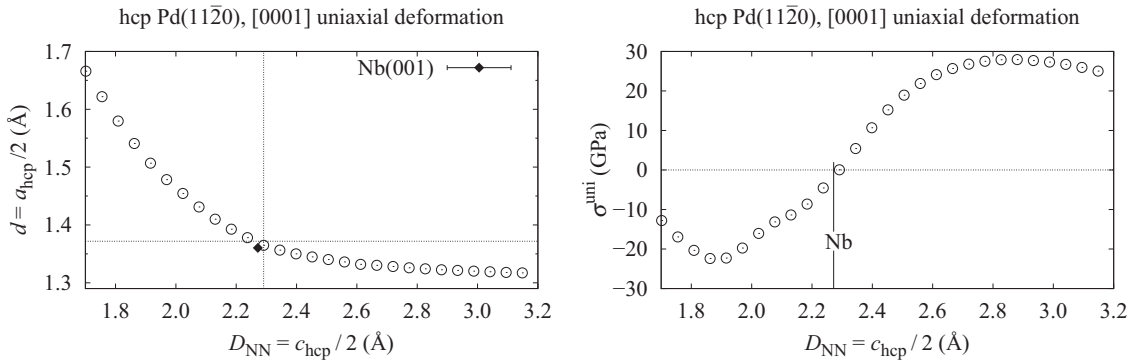

FIG. 7. The interlayer distances d (left) and epitaxial stresses σ^{epi} (right) of hcp Pd films with the (11$\bar{2}$0) geometry on bcc(001) substrates as functions of the nearest-neighbor distance D_{NN} in the plane of the film. Let us note that in this case we approximate the epitaxial stress in the plane (11$\bar{2}$0) by the uniaxial stress in the direction [0001] [see Fig. 1(c)].

$c/a = 1.68$ ratio for hcp Pd and corresponds to the film with $D_{NN} = 2.18$ Å and $d = 1.39$ Å and a compressive epitaxial stress equal to -8.7 GPa. This is about 39% of the maximum attainable value for hcp Pd films.

LDA (without volume correction) yields the atomic volume for hcp Pd equal to 14.232 Å^3/atom (see Fig. 3). If the volume correction is applied, then the equilibrium atomic volume becomes 14.777 Å^3/atom. This is about 0.5% higher atomic volume than the fcc experimental volume. The c/a ratio is 1.68. On the basis of the RHEED information on Pd admetal films that are grown on a Nb(001) substrate [70] one is led to a conclusion that the Pd film lattice constant is by 1% smaller than that of the bulk fcc Pd and that the experimental c/a ratio for hcp(11$\bar{2}$0) films is 1.67 (see Figs. 10 and 11). This corresponds to the lattice parameters $a_{hcp} = 2.721$ Å and $c_{hcp} = 4.543$ Å (Fig. 7). It is a result of a fact that the atomic density of the Pd admetal is conserved; i.e., it keeps its bulk (fcc) value [70]. As seen in Fig. 1(c), the two lattice parameters, $a_{hcp}\sqrt{3} \approx 1.73 a_{hcp}$ and $c_{hcp} = 1.68 a_{hcp}$, should somehow fit the square symmetry of the underlying bcc(001) Nb substrate. Unfortunately, the experimental hcp structure of Pd grown on the Nb(001) substrate is out of the ferromagnetic region depicted in Fig. 11. As a result, we predict that the hcp Pd films grown on the Nb substrate should not be ferromagnetically ordered. The question arises if ferromagnetism can be achieved in those films by some technological route. For its finding let us further discuss experimental facts and other theoretical predictions about the hcp structure of Pd.

The hcp structure of Pd is not the ground-state structure. It can be regarded as a disturbed fcc stacking of (111) atomic planes with a vast number of stacking faults inserted into the initial *ABC* stacking to become an *ABAB* stacking [75]. Existence of a higher magnetic moment in the hcp phase of Pd corresponds to a previous theoretical prediction that fcc Pd increases its overall magnetic moment with increasing number of stacking faults [25]. We note that the hcp structure exhibits channels of free space along the [0001] direction. There is a reduced coordination number along these channels. A similar prediction of ferromagnetic ordering for hcp and dhcp Pd films has been made and indirectly confirmed by experiment in Ref. [9]. Similarly, ferromagnetic ordering has been theoretically predicted in coaxial Pd nanowires [41]. Experimentally, the Pd clusters and nanoparticles have been confirmed to be ferromagnetic [24,76–78].

Further, the ferromagnetism of hcp Pd is favored by fulfilling the Stoner criterion for ferromagnetism [9,25]. The paramagnetic density of states (DOS) of hcp Pd presented in Ref. [25] yields the value at the Fermi energy equal to $N(E_F) = 2.86$ states/atom/eV (the authors report the value of 1.43 states/atom/eV per spin). It is important to point out that this quite a high value of $N(E_F)$ has been calculated for hcp structure with the ideal ratio of lattice constants $c_{hcp}/a_{hcp} = \sqrt{8/3} \approx 1.633$. A similar value of 2.70 states/atom/eV [9] has been reported earlier. The value of exchange integral for hcp Pd [79] is $I = 0.71$ eV. It is somewhat higher than the exchange integral for fcc Pd $I = 0.626$ eV provided in Ref. [80]. [In that work, the authors report the value of 0.023 Ry = 0.313 eV, which is meant to be multiplied by the total density of states for both spins. However, here we keep the usual convention for Stoner criterion dealing with the product $IN(E_F)$, where $N(E_F)$ is the DOS per spin.] Using the above-mentioned data, the product $IN(E_F)$ lies between 0.959 and 1.015.

The point of our interest is the transition between nonmagnetic and ferromagnetic hcp Pd structure as it can be seen along the uniaxial deformation path in Fig. 11. In order to discuss more thoroughly this phenomenon, we calculated the DOS for the equilibrium configuration corresponding to the experimental value of $c_{hcp}/a_{hcp} = 1.68$ and next two points (squares) to the left (Fig. 13). They correspond to uniaxially deformed hcp Pd along the [0001] axis with Poisson contraction (here rather extension) included at $\epsilon = -2.34\%$ and -4.68% ($c_{hcp}/a_{hcp} = 1.62$ and 1.57, respectively). The uncompressed hcp Pd has the DOS at Fermi level equal to $N(E_F) = 2.50$ states/atom/eV (1.25 states/atom/eV per spin). After uniaxial compression along the [0001] axis the DOS at Fermi level increases first to 3.00 states/atom/eV for deformation of $\epsilon = -2.34\%$ and then even to 3.15 states/atom/eV for deformation of $\epsilon = -4.68\%$ at the plateau corresponding to the magnetic moment of 0.3 μ_B in Fig. 11. It is seen that the product $IN(E_F)$ increases from 0.888 through 1.065 to 1.115. The Stoner criterion $IN(E_F) \geqslant 1$ thus confirms the nonmagnetic to ferromagnetic transition during compression along the uniaxial deformation path as the total energy of the nonmagnetic state with constrained equal density of both spin-up and spin-down populations is lowered as soon as this

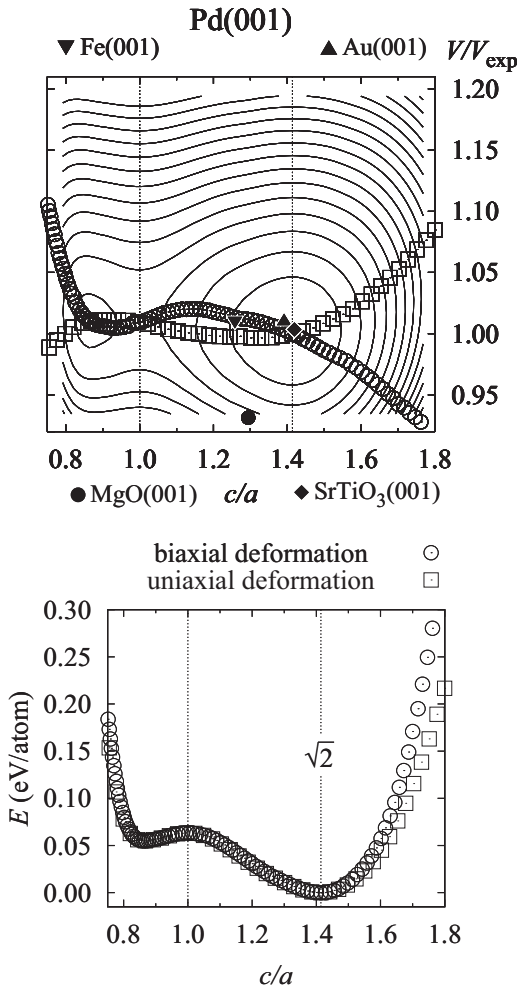

FIG. 8. (Top) Total energy E of tetragonally deformed Pd as a function of the ratio of lattice constants c/a and the relative atomic volume V/V_{exp}. This geometry corresponds to Pd films grown on the (001) substrates. Circles and squares show the biaxial (interlayer distance d relaxed) and uniaxial (nearest-neighbor distance D_{NN} relaxed) deformation paths [20–23,35–37]. (Bottom) Total-energy profiles along the biaxial (circles) and uniaxial (squares) deformation paths. Vertical lines mark the bcc ($c/a = 1$) and fcc ($c/a = \sqrt{2}$) structures.

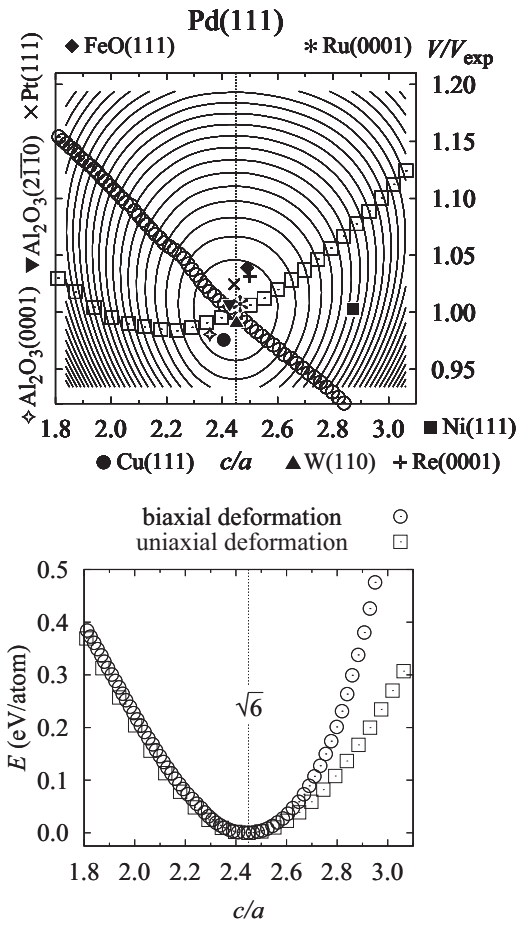

FIG. 9. (Top) Total energy E of trigonally deformed Pd as a function of the ratio of lattice constants c/a and the relative atomic volume V/V_{exp}. This geometry corresponds to Pd films grown on the (111) substrates. The meanings of circles and squares are the same as in Fig. 8. (Bottom) Total-energy profiles along the biaxial (circles) and uniaxial (squares) deformation paths. Vertical line marks the fcc structure ($c/a = \sqrt{6}$).

constraint is removed. As a result, a ferromagnetic ordering occurs.

Figures 3 and 12 indicate that the ferromagnetic energy gain in the Pd films $E_{\text{NM}} - E_{\text{FM}}$ is very small (0–5 meV/atom) and thus a small perturbation introduced by phonons at elevated temperature may break the ferromagnetic ordering. A rough estimate of Curie temperature of hcp Pd is below 58 K according to the relation $\Delta E = k\Delta T$. This indicates a possibility to use hcp Pd films as sensors in cryogenic technology.

Provided that the hcp Pd is not deformed except of increase in volume, Fig. 12 reveals that the ferromagnetic ordering of hcp Pd starts to be favored at higher atomic volumes than the experimental one. The same situation arises for the magnetic moment that is between 0.0 and 0.4 μ_{B}/atom for atomic volumes greater than the experimental one.

It is interesting to compare these values with those corresponding to the bcc modification of the $3d$ metal Ni (isoelectronic to Pd). It is known that bcc Ni prefers ferromagnetic ordering to nonmagnetic [22]. At the experimental atomic volume, the ferromagnetic energy gain of bcc Ni amounts to 16 meV/atom and its magnetic moment reaches 0.55 μ_{B}/atom.

If one considers the hcp Pd structure to be only a different AB stacking of the corresponding (111) atomic layers that are present in the fcc structure, one should obtain the ideal hcp ratio $c/a = \sqrt{8/3} \approx 1.633$. However, a larger experimentally measured c/a ratio (1.67) of hcp Pd films indicates that the distance between layers $c_{\text{hcp}}/2$ in (0001) Pd film exceeds the distance of the (111) layers in bulk fcc Pd. Obviously, a larger c/a value yields a unit cell in the hcp$(11\bar{2}0)$ plane of the hcp lattice which is closer to a square and hence fits better onto the square mesh of the (001) surface of the substrate. It has been already predicted in Ref. [43] that this larger c/a reflects a bulk property of an hcp Pd phase and it is not caused exclusively by epitaxial stress in hcp films.

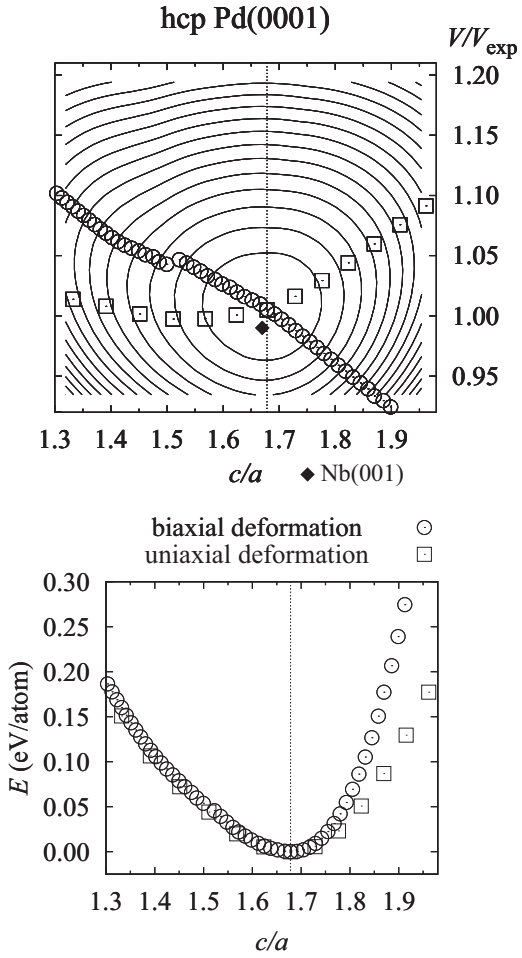

FIG. 10. (Top) Total energy E of uniaxially deformed hcp Pd along the [0001] axis as a function of the ratio of lattice constants c/a and the relative atomic volume V/V_{exp}. This geometry corresponds to hcp(11$\bar{2}$0) Pd films grown on bcc(001) substrates. The meaning of circles and squares is the same as in Fig. 8. (Bottom) Total-energy profiles along the biaxial (circles) and uniaxial (squares) deformation paths. Vertical line marks the equilibrium hcp structure ($c/a = 1.68$).

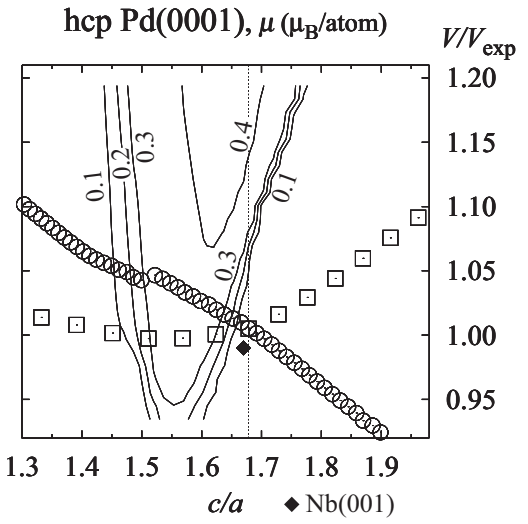

FIG. 11. Magnetic moment μ of atoms in hcp(11$\bar{2}$0) Pd films grown on the bcc(001) substrates as a function of the ratio c/a and the relative atomic volume V/V_{exp}. The circles show the biaxial deformation path and squares represent uniaxial deformation path along the hcp [0001] direction. A vertical line marks the equilibrium hcp structure ($c/a = 1.68$).

Therefore, we propose a technology of fabricating ferromagnetic Pd films grown on Nb(001) or W(001) substrate [9]. First, the domain structure of the hcp Pd film [43] should be moderated in such a way that one direction in the bcc substrate (for example the [110] direction) is selected as the main direction. All hcp(11$\bar{2}$0) islands with the hexagonal [0001] axis lying along this direction should be left on the substrate. The remaining islands should be removed. Next, a uniaxial compression in the [110] direction of the bcc substrate should be applied. After compressing the bcc substrate and the hcp Pd islands together along their [0001] direction by about 6.3%, one should reach the hcp $c/a = 1.564$ ratio of hcp Pd films. Then, the magnetic properties of those films can be measured by a suitable experimental method. There is an indirect evidence of the ferromagnetic ordering in such hcp Pd structures and this is the experimental observation of ferromagnetic behavior of fcc twinned Pd particles [78]. The twins can induce stacking faults [25,81] in the overall *ABC* stacking of the fcc structure in a Pd nanoparticle. The spacing between the (111) atomic layers of the fcc structure is equivalent to the spacing between the hcp(0001) layers that is achieved for the ideal hcp $c/a = 1.633$ ratio. According to Fig. 11, this hcp c/a ratio occurs already in the region of the onset of ferromagnetism.

Moreover, a careful analysis of the strains present in the (111) interlayer spacings in fcc twinned Pd nanoparticles [24] indicates that these strains contribute to the magnetic moment due to inner ferromagnetism of the Pd particle. The strains are caused mainly due to the surface stress. It is noteworthy to point out that Ref. [24] presents the mean value of the strain ϵ to be negative. On the other hand, the authors of Ref. [24] conclude from previous theoretical studies (e.g., Refs. [9,76]) that negative strains do not lead to the appearance of ferromagnetism in Pd. However, our results put this theoretical assumption under further consideration.

Let us consider some neighborhood of a twin boundary in the Pd nanoparticle, where the *ABC* stacking of the fcc(111) layers is locally perturbed [25,81]. Usually, the stacking of fcc(111) layers at the twin boundary need not be exactly of the type of *AB* (Ref. [81]) corresponding to the hcp structure, but we can use the hcp model as a first approximation of a locally perturbed stacking of the fcc(111) layers. In our model, a decrease of the interlayer distance d_{111} suggested by Ref. [24] corresponds to a compression along the [0001] direction of the local hcp Pd structure. This deformation is illustrated in Fig. 11 as the path corresponding to a uniaxial deformation path (open squares). It is seen there that the atomic volume of the local hcp configuration should decrease a little bit. Further, the distance of atoms in the (0001) hcp plane increases with the decreasing c/a hcp ratio. What is most significant, the reduction of the ideal hcp ratio (1.633) by about 4.23% leads to $c/a = 1.564$, a point in the uniaxial deformation path that lies in the middle of the ferromagnetic

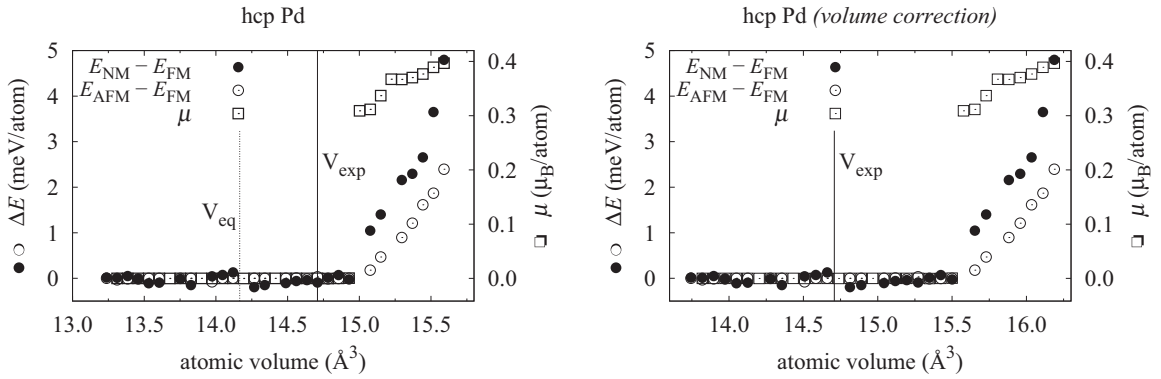

FIG. 12. (Left) Volume variation of the energy differences between NM, AFM, and FM states ΔE (ΔE is taken with respect to the ferromagnetic state: $\Delta E_{\mathrm{NM}} = E_{\mathrm{NM}} - E_{\mathrm{FM}}$ and $\Delta E_{\mathrm{AFM}} = E_{\mathrm{AFM}} - E_{\mathrm{FM}}$) and volume variation of the magnetic moment μ for hcp Pd. The ratio of lattice parameters c/a has been relaxed for each volume. The full vertical line denotes the experimental atomic volume; the dotted vertical line corresponds to calculated equilibrium volume. (Right) The same after the *volume correction*.

region depicted in Fig. 11 and characterized by the value of magnetic moment of 0.3 μ_{B}. Moreover, even strains $\epsilon = (d\{111\}_{\mathrm{nanoparticle}} - d\{111\}_{\mathrm{bulk}})/d\{111\}_{\mathrm{bulk}}$ lower in magnitude than -1.34% that have been measured in Ref. [24] cause the hcp structure to be compressed so that the c/a ratio attains a value of 1.611. The point on the uniaxial deformation path exhibiting this c/a ratio also lies on the plateau with the magnetic moment of 0.3 μ_B per atom (Fig. 11). We conclude that it is a very fortuitous coincidence that the ferromagnetism in the twins present in a fcc Pd nanoparticle is supported by a strain lower in magnitude than -1.34%. According to the LDA calculations, such a small value of negative strain in the interlayer distance $d_{\{111\}}$ is sufficient to enhance ferromagnetic behavior of the local hcp structure present in the neighborhood of the twins. In this way, the ferromagnetism induced by small strains in Pd nanoparticles is explained.

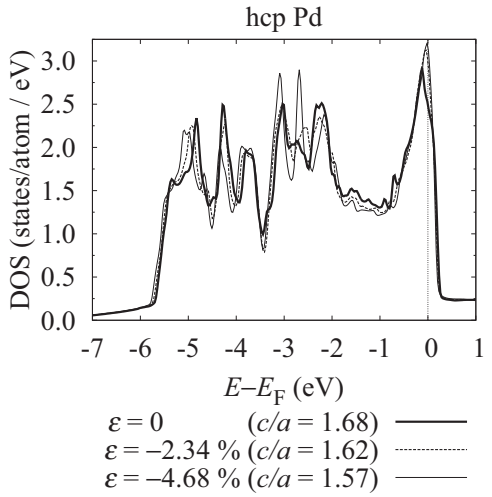

FIG. 13. Calculated density of states of non-magnetic hcp Pd at first three points of the uniaxial deformation path corresponding to a compression along the [0001] axis (and to a decrease of the ratio of hexagonal lattice constants c/a; Poisson contraction—here rather an extension—is included). In the calculation, the equal spin-up and spin-down populations have been kept. The thick line denotes DOS at the experimental ratio of hexagonal lattice constants; the dotted line and the thin line denote DOS for uniaxially deformed hcp structures.

Table IV presents the c/a ratio of bct lattice parameters, deviation of the atomic volume of the Pd film from the experimental value of fcc Pd and epitaxial stress in Pd films grown on the Nb(001) [8,13], W(001) [7,11], and V(001) [57] substrates. All mentioned bct Pd films are found up to the thickness of two monolayers. The Pd film on V(001) starts to grow in its natural fcc phase after two monolayers of pseudomorphic growth. In contrast, the Pd films on the Nb(001) and W(001) substrates start to grow in the hcp phase after two monolayers of pseudomorphic growth. This coincides with the fact that bct Pd film on V(001) substrate exhibits the $c_{\mathrm{bct}}/a_{\mathrm{bct}}$ ratio higher than 1 and bct Pd films on Nb(001) and W(001) substrates exhibit the $c_{\mathrm{bct}}/a_{\mathrm{bct}}$ ratio lower than 1.

In the plot of epitaxial stress presented in Fig. 5 we have found two more structures with zero epitaxial stress apart from the fcc Pd with $D_{\mathrm{NN}} = 2.75$ Å. The first one is the bcc Pd with $a_{\mathrm{bcc}} = D_{\mathrm{NN}} = 3.098$ Å (see Fig. 5). The second one is the bct structure corresponding to the $D_{\mathrm{NN}} = 3.251$ Å and $d = 1.4056$ Å. The ratio of bct lattice parameters in this case yields $c/a = 0.865$.

Furthermore, the epitaxial stress σ^{epi} in Fig. 5 is very low in the range between $D_{\mathrm{NN}} = 3.05$ Å and $D_{\mathrm{NN}} = 3.30$ Å. Consequently, it can be expected that a lot of bct Pd films can be grown there on bcc(001) substrates by the pseudomorphic growth. However, the experiment shows [7,8,11–13] that for Pd films thicker than two monolayers, hcp Pd grows. So Fig. 5 shows that it can be expected that the epitaxial hcp Pd is a very stable system, for although bct Pd should have low epitaxial stress, it does not appear (for films thicker than two monolayers). To illustrate this, let us compare the epitaxial stress for the bct(001) Pd and the hcp(11$\bar{2}$0) Pd grown on the Nb(001) substrate. The bct(001) Pd film yields $\sigma^{\mathrm{epi}} = 2.35$ GPa (Fig. 5) but the hcp(11$\bar{2}$0) Pd yields even a lower value of $\sigma^{\mathrm{epi}} = -1.60$ GPa (Fig. 7).

It is seen from Fig. 18 that the ferromagnetic energy gain ΔE_{NM} in bcc Rh is very small. Namely, it amounts to 1.5 meV/atom at the equilibrium atomic volume and 2.2 meV/atom at the experimental atomic volume. The corresponding magnetic moments are 0.24 and 0.28 μ_{B}/atom, respectively. A small value of ferromagnetic energy gain

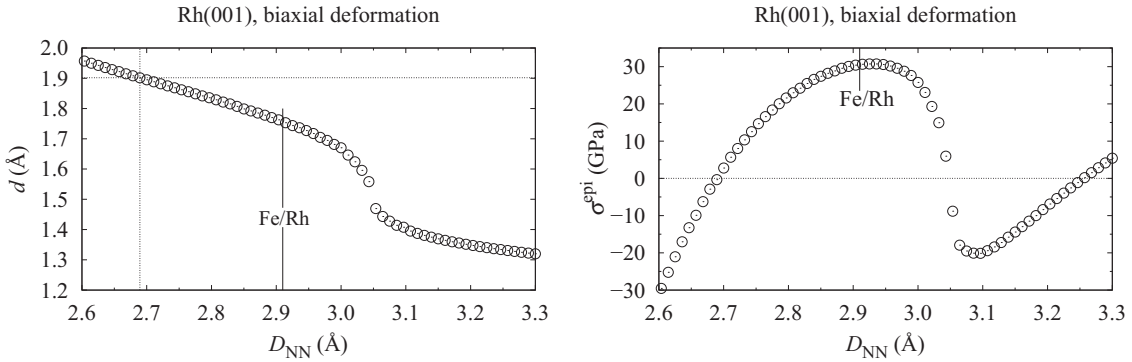

FIG. 14. The interlayer distances d (left) and epitaxial stresses σ^{epi} (right) of Rh films grown on (001) substrates as functions of the nearest-neighbor distance D_{NN} in the plane of the film. The dotted lines denote the values of d and D_{NN} for experimentally determined fcc structure of Rh (left) and zero epitaxial stress (right).

contrasts with the value of ΔE_{NM} for the fcc modification of the 3d metal Co that is isoelectronic to Rh. Fcc Co at the experimental volume favors ferromagnetism [22] and the ferromagnetic energy gain amounts to 214 meV/atom. This is two orders of magnitude higher than the case of the bcc modification of the 4d metal Rh. The corresponding magnetic moment for fcc Co equals 1.66 μ_B/atom.

A high disproportion between the ΔE_{NM} in fcc Co and bcc Ni on one hand and in bcc Rh and hcp Pd on the other hand indicates one feature of magnetism in 4d metals. Namely, if these 4d metals are found to be ferromagnetic in some higher-energy structure, they should have a very low Curie temperature compared to the case of 3d ferromagnetic metals.

The bct Rh films have been grown in a form of Rh(001)/Fe(001) multilayers [14]. As these experimental results provide an important check of our predictions, we study this system in detail. First, it is seen from Fig. 14 that the zero epitaxial stress corresponds to the in-plane distance D_{NN} of 3.0473 Å. This means that on a substrate with a D_{NN} close to this value a bcc structure can be grown. The atomic volume of the bcc structure is 14.148 Å^3/atom. This is by about 2.86% more than is the experimental atomic volume of fcc Rh (see Figs. 4, 16, and 19). LDA yields equilibrium atomic volume of bcc Rh as 13.658 Å^3 (see Fig. 4). After applying the volume correction, this equilibrium atomic volume becomes 14.161 Å^3/atom.

Our bcc Rh lattice constant calculated within the LDA and with the volume correction included equals $a_{bcc} = 3.047$ Å and is by 1.7% lower than the experimental value of $a_{bcc} = 3.10$ Å provided in Ref. [14] and by 2.0% lower than the theoretical result 3.11 Å calculated using the generalized gradient approximation for exchange-correlation energy [10]. However, the upper part of Fig. 16 explains why bcc Rh cannot be stabilized in the form of thin films, because it represents a saddle point at the tetragonal ratio $c/a = 1.0$ in the total-energy profile.

Second, it is seen from Fig. 14 that there is a bct Rh structure with zero epitaxial stress at $D_{NN} = a_{bct} = 3.256$ Å. The corresponding interlayer distance is very low, $d = 1.331$ Å, and the ratio of bct lattice parameters for this structure is $c/a = 0.818$. This bct Rh structure corresponds to the local minimum in Fig. 16.

Third, the in-plane lattice parameter for the Rh/Fe superlattice in a sample of {MgO(100)/Fe40 Å/[Rh 3 Å/Fe 10 Å]$_{20}$ Al 20 Å} [14] is $D_{NN} = 2.91$ Å. The authors have given the value of D_{NN} only for the sample with Rh thickness $t_{Rh} = 3$ Å. Further, the measured out-of-plane period of such superlattice is 12.3 Å. Assuming the in-plane distance D_{NN} to be fixed for both Rh and Fe layers and using the estimates given

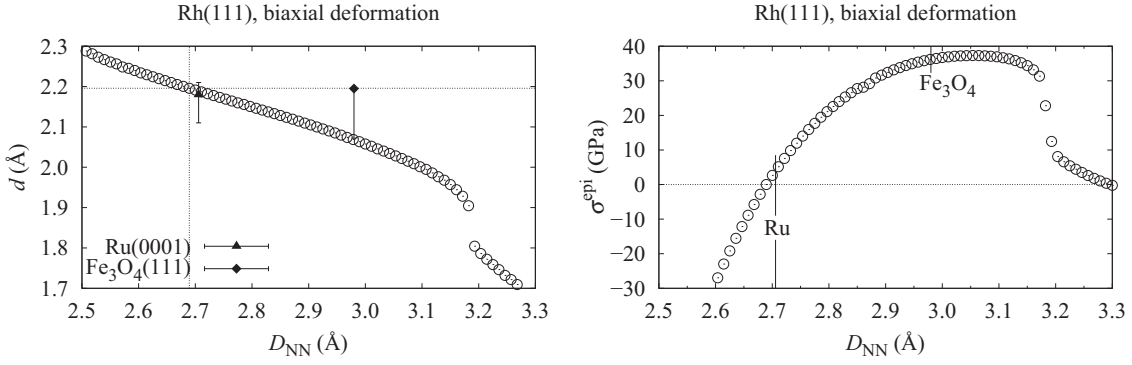

FIG. 15. The interlayer distances d (left) and epitaxial stresses σ^{epi} (right) of Rh films grown on the fcc(111) substrates as functions of the nearest-neighbor distance D_{NN} in the plane of the film. The dotted lines denote the values of d and D_{NN} for experimentally determined fcc structure of Rh (left) and zero epitaxial stress (right). The error bars show the variance of d measured in the Rh(111) films with various thicknesses.

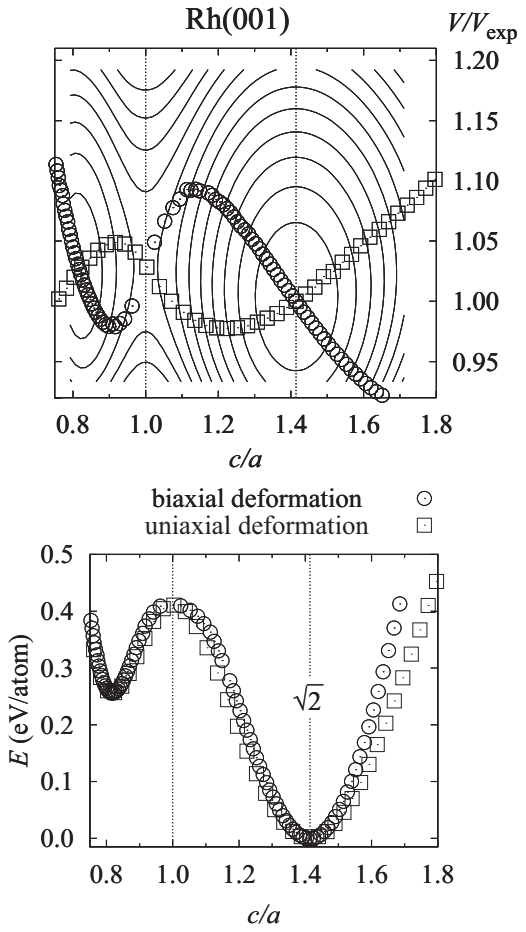

FIG. 16. (Top) Total energy E of tetragonally deformed Rh as a function of the ratio of lattice constants c/a and the relative atomic volume V/V_{exp}. This geometry corresponds to Rh films grown on the (001) substrates. The meanings of circles and squares are the same as in Fig. 8. (Bottom) Total-energy profiles along the biaxial (circles) and uniaxial (squares) deformation paths. Vertical lines mark the bcc ($c/a = 1$) and fcc ($c/a = \sqrt{2}$) structures.

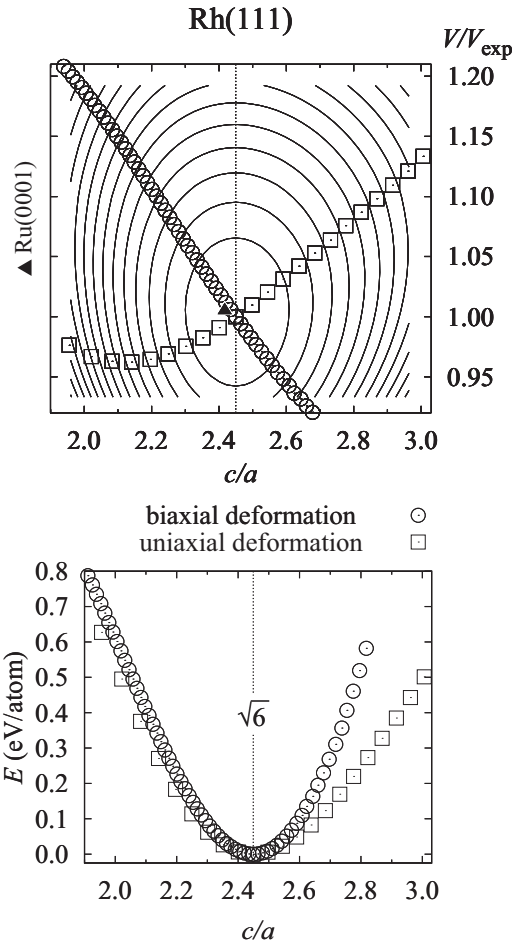

FIG. 17. (Top) Total energy E of trigonally deformed Rh as a function of the ratio of lattice constants c/a and the relative atomic volume V/V_{exp}. This geometry corresponds to Rh films grown on the (111) substrates. The meanings of circles and squares are the same as in Fig. 8. (Bottom) Total-energy profiles along the biaxial (circles) and uniaxial (squares) deformation paths. Vertical line marks the fcc structure ($c/a = \sqrt{6}$).

in Fig. 14 and in Refs. [20,82], we conclude that at this unique D_{NN}, the interlayer distance $d_{\text{Rh-Rh}}$ of Rh is 1.757 Å and the interlayer distance of Fe is $d_{\text{Fe-Fe}} = 1.412$ Å. The Rh layers in the superlattice form a bct structure with the ratio of lattice parameters $c/a = 1.208$. The value of Rh interplanar spacing $d_{\text{Rh-Rh}} = 1.757$ Å is by about 3.5% lower than the estimate of $d_{\text{Rh-Rh}} = 1.82$ Å provided in Ref. [14]. Let us note that this estimate has assumed conservation of the atomic volume (referred to the bcc structure with $a_{\text{bcc}} = 3.10$ Å). If one assumes conservation of the bcc atomic volume in the case where a_{bcc} equals to our calculated value of 3.047 Å, then the estimate of interlayer distance d is only 1.671 Å. It further disagrees by 4.9% with the value of $d_{\text{Rh-Rh}}$ determined from Fig. 14 and this discrepancy may be explained by an enhancement of atomic volume in the region between the bcc and fcc structure on the curve exhibiting biaxial deformation path illustrated in Fig. 16.

We propose a suitable structural model assuming that there are three monolayers of Rh in the Rh/Fe superlattice. Their overall thickness of 3.514 Å is somewhat bigger than the 3 Å given in the sample composition. Further, the three Rh monolayers are followed by five monolayers of Fe. Their thickness of 5.648 Å sums up with the Rh thickness to 9.162 Å. The missing length of 3.138 Å up to the lattice period 12.3 Å is filled by two interfaces between Rh and Fe monolayers. We thus conclude that the distance between the Rh layers and Fe layers $d_{\text{Rh-Fe}}$ is 1.569 Å. This number lies in between the $d_{\text{Rh-Rh}}$ and $d_{\text{Fe-Fe}}$.

TABLE IV. Calculated ratio of lattice parameters $c_{\text{bct}}/a_{\text{bct}}$, relative change of atomic volume ΔV and the epitaxial stress σ^{epi} of bct Pd on bcc substrates.

Substrate	$c_{\text{bct}}/a_{\text{bct}}$	ΔV (%)	σ^{epi} (GPa)
Nb(001)	0.835	+2.0	2.35
W(001)	0.932	+0.5	−1.32
V(001)	1.076	+1.8	3.09

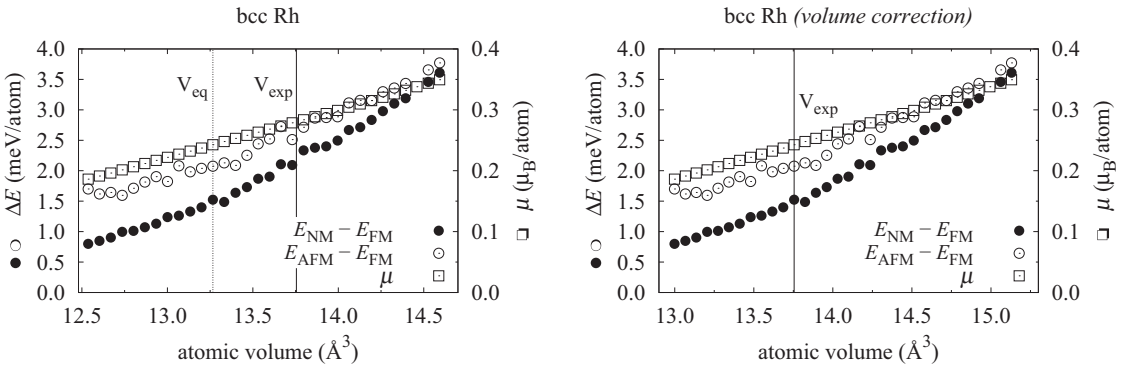

FIG. 18. (Left) Volume variation of the energy differences between NM, AFM, and FM states ΔE (ΔE is taken with respect to the ferromagnetic state: $\Delta E_{NM} = E_{NM} - E_{FM}$ and $\Delta E_{AFM} = E_{AFM} - E_{FM}$) and volume variation of the magnetic moment μ for bcc Rh. The full vertical line denotes the experimental atomic volume; the dotted vertical line corresponds to calculated equilibrium volume. (Right) The same after the *volume correction*.

However, some questions arise as the measured out-of-plane lattice parameter is 2.99 ± 0.01 Å and it corresponds to a double average interlayer distance d of 1.495 Å. Simply multiplying this number by 8 yields the superlattice period of only 11.96 Å. This is lower than the measured superlattice period of 12.3 Å. This discrepancy can be explained if the model is altered in such a way that one allows for the variance of the in-plane distance D_{NN} throughout the Fe/Rh supercell. In such a model, the value of in-plane spacing D_{NN} is only an *average* value in the Fe/Rh supercell and it should vary with the Rh thickness similarly as the average interplanar spacing d varies with Rh thickness [14]. We point out that all the experimental findings given in Ref. [14] are valid for Rh films that are only several monolayers thick. However, as the bulk calculations were successfully used for determining electronic structure of thin films and overlayers [20–23], they also present a good first approximation in this case.

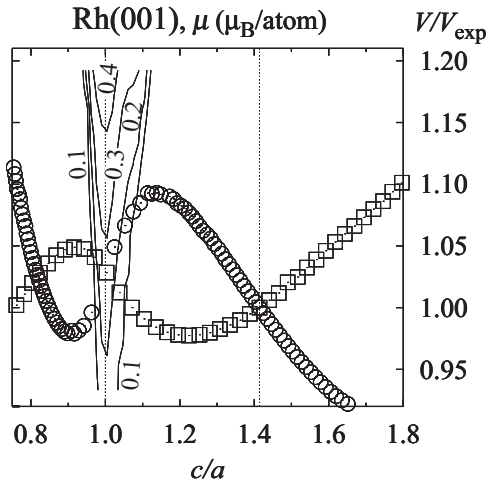

FIG. 19. Magnetic moment μ of atoms in Rh films grown on the (001) substrates as a function of the ratio c/a and the relative atomic volume V/V_{exp}. The circles show the biaxial deformation path and squares represent the uniaxial deformation path. Vertical lines mark the bcc ($c/a = 1$) and fcc ($c/a = \sqrt{2}$) structures.

The average d runs through the range between $d = 1.46$ Å for the Rh thickness $t_{Rh} = 1.50$ Å and $d = 1.80$ Å for $t_{Rh} = 6.0$ Å [14]. The Rh thickness of 1.50 Å corresponds roughly to two monolayers. The value of d in this case is by about 2.3% lower than the value $d = 1.495$ Å reported for $t_{Rh} = 3$ Å corresponding roughly to three Rh monolayers. (The authors of Ref. [14] do not indicate the error values here). Moreover, if a critical Rh thickness t_{crit} is reached at $t \approx 5$ Å for this sample, then a transition occurs from a bct structure to the fcc structure in the Rh/Fe supercell. These facts indicate that the region of bct Rh close to a rapid drop of d in Fig. 14 could be reached in the Rh layers present in the Fe/Rh multilayers.

The appearance of ferromagnetic ordering in bcc Rh shown in Fig. 19 may be further verified by analyzing the Stoner criterion of ferromagnetism [80]. The shape of the density of states in bcc Rh in paramagnetic state may be found in Ref. [18]. The value of $N(E_F)$ calculated there using the LDA amounts to 3.9 states/atom/eV. Our calculation yields somewhat lower value of 3.16 states/atom/eV. This corresponds to 1.58 states/atom/eV per spin. On the other hand, an older calculation in Ref. [80] reports the value of only 0.905 states/atom/eV per spin and the exchange parameter $I = 0.631$ eV (again, we double the value of 0.0232 Ry = 0.316 eV reported by those authors in order to obtain a value of I that can be multiplied by the DOS per spin). Using the value of $N(E_F)$ provided by our calculations, the product $I\,N(E_F)$ amounts to 0.997. It indicates that, according to the Stoner criterion, bcc Rh is on the verge of ferromagnetism.

The authors of the experimental study of Rh(001)/Fe(001) multilayers [14] report two distinct regions of Rh films. The Rh layers in the composed films were ferromagnetic when the structure was bct and nonmagnetic when the structure was fct. This is in a good agreement with Fig. 19. The region of ferromagnetism there lies in the range between $c_{bct}/a_{bct} = 0.97$ and 1.07. Their equivalents in Fig. 14 correspond to $D_{NN} = 3.054$ Å, $d = 1.470$ Å, $\sigma^{epi} = -9.0$ GPa and the other point to $D_{NN} = 3.021$ Å, $d = 1.625$ Å, $\sigma^{epi} = +19.4$ GPa. There is a change of atomic volume between the two points: from 13.710 to 14.837 Å^3/atom; i.e., the relative change of atomic volume with respect to the atomic volume of the bcc Rh structure changes from -3.1% to $+4.9\%$. (This corresponds

to a relative change of atomic volume with respect to the Rh ground-state fcc structure from +0.3% to +7.9%.) This volume change may be the cause of a very high epitaxial stress in the bct Rh illustrated in Fig. 14.

The experimentally reported values of magnetic moments present on Rh atoms in Ref. [14] were between zero and 1.5 μ_B/atom, indicating that the magnetism of Rh atoms is primarily due to the proximity of Fe atoms. However, the authors also conclude that the ferromagnetic state of Rh is partly stabilized by its bct structure. This is further supported by the results presented in Fig. 19. There the intersection of biaxial deformation path (open circles) with the contours of nonzero magnetic moments is found for values of magnetic moment between 0.1 and 0.3 μ_B/atom.

V. CONCLUSIONS

We have studied several crystal structures of Pd and Rh thin films by means of *ab initio* calculations. We have employed the bulk model of the film provided that some constraint was applied to the structure. This constraint was a fixed in-plane distance of nearest-neighbor atoms. The perpendicular interlayer distance d was relaxed so that a particular d was determined from the minimum of the total energy E with respect to the d. Dependencies of d on nearest-neighbor distance D_{NN} in the plane of the film parallel to the substrate have been obtained and epitaxial stresses were calculated for a set of the D_{NN} values in the film. Our calculated results for biaxial (and additionally uniaxial) deformation paths have been plotted in contour plots of total energy as a function of ratio of (tetragonal or hexagonal) lattice constants c/a and the relative atomic volume.

Further, magnetic properties of the bulk Pd and Rh were investigated and similar contour plots of atomic magnetic moment as a function of c/a and V/V_{exp} have been drawn.

Our LDA calculations predict hcp Pd to be on the verge of ferromagnetic ordering. The hcp c/a ratio of (bulk) hcp Pd is 1.68. In order to start the ferromagnetic onset in hcp Pd, for example in hcp(11$\bar{2}$0) Pd films, one needs to decrease the c/a ratio of hexagonal lattice parameters so that it is close to 1.564. This value is about 6% lower than the experimentally observed value 1.67. This result allows us to explain the experimental findings of ferromagnetic ordering induced by strain in twinned Pd nanoparticles assuming that the local structure at the twin boundaries can be modeled by a local *AB* stacking of fcc(111) atomic planes with a reduced c/a ratio of a local hcp structure. We also predict the hcp Pd films grown on the Nb(001) substrate not to be ferromagnetically ordered.

On the other hand, we have found that bcc Rh should be ferromagnetic. The bcc structure represents a saddle point in the dependence of the total energy on the tetragonal ratio c/a and atomic volume. Therefore, it cannot be stabilized in the form of thin films. However, a slightly biaxially deformed bcc structure (the ratio of bct lattice parameters c/a ranging between 0.97 and 1.07) can still retain a nonzero magnetic moment.

ACKNOWLEDGMENTS

This research has been financially supported by the Ministry of Education, Youth and Sports of the Czech Republic under the Project CEITEC 2020 (Project No. LQ1601), by the Academy of Sciences of the Czech Republic (Institutional Project No. RVO:68081723), and by the Czech Science Foundation (Project No. GA16-24711S). E.H. was supported by the Deutsche Forschungsgemeinschaft (DFG) under Contract No. HU 2170/2-1. Computational resources were supplied by the Ministry of Education, Youth and Sports of the Czech Republic under the Projects CESNET (Project No. LM2015042), CERIT-SC (Project No. LM2015085), and IT4Innovations (Project No. LM2015070) provided under the program "Projects of Large Research, Development and Innovations Infrastructures."

[1] W. Yourgrau and S. Mandelstam, *Variational Principles in Dynamics and Quantum Theory* (Dover Publications, New York, 2007).

[2] A. Grünebohm, P. Entel, and C. Ederer, First-principles investigation of incipient ferroelectric trends of rutile TiO_2 in bulk and at the (110) surface, Phys. Rev. B **87**, 054110 (2013).

[3] M. Marathe and C. Ederer, Electrocaloric effect in $BaTiO_3$: A first-principles-based study on the effect of misfit strain, Appl. Phys. Lett. **104**, 212902 (2014).

[4] K. Dymkowski and C. Ederer, Strain-induced insulator-to-metal transition in $LaTiO_3$ within DFT+DMFT, Phys. Rev. B **89**, 161109 (2014).

[5] J. Tsuji, *Palladium Reagents and Catalysts: New Perspectives for the 21st Century* (John Wiley & Sons, Chichester, 2004).

[6] *Modern Rhodium-Catalyzed Organic Reactions*, edited by P. A. Evans (Wiley-VCH, Weinham, 2005).

[7] H. Wormeester, E. Hüger, and E. Bauer, hcp and bcc Cu and Pd Films, Phys. Rev. Lett. **77**, 1540 (1996).

[8] H. Wormeester, E. Hüger, and E. Bauer, Importance of the Surface Electronic Structure in Heteroepitaxy, Phys. Rev. Lett. **81**, 854 (1998).

[9] E. Hüger and K. Osuch, Ferromagnetism in hexagonal close-packed Pd, Europhys. Lett. **63**, 90 (2003).

[10] C. Paduani, Band structure and Fermi surfaces of alternate structural phases of Co and Rh, Solid State Commun. **152**, 28 (2012).

[11] H. Wormeester, E. Hüger, and E. Bauer, Growth and electronic structure of thin epitaxial Pd and Co films on W(100), Phys. Rev. B **54**, 17108 (1996).

[12] J. Brona and A. Ciszewski, Structural and compositional changes of the ultrathin Pd layers on Nb(001) caused by annealing, Appl. Surf. Sci. **222**, 432 (2004).

[13] E. Hüger and K. Osuch, Pd bonded on Nb(001): Dependence of noble metal and ferromagnetic characteristics on film thickness, Phys. Rev. B **72**, 085432 (2005).

[14] M. A. Tomaz, D. C. Ingram, G. R. Harp, D. Lederman, E. Mayo, and W. L. O'Brien, Fe/Rh (100) multilayer magnetism probed by x-ray magnetic circular dichroism, Phys. Rev. B **56**, 5474 (1997).

[15] M. Všianská and M. Šob, The effect of segregated sp-impurities on grain-boundary and surface structure, magnetism and embrittlement in nickel, Prog. Mater. Sci. **56**, 817 (2011).

[16] H. Li, S. C. Wu, D. Tian, Y. S. Li, J. Quinn, and F. Jona, Ultrathin films of Rh on Au{001} and Rh on Ag{001}: Growth mode and magnetism, Phys. Rev. B **44**, 1438 (1991).
[17] T. Kachel, W. Gudat, C. Carbone, E. Vescovo, S. Blügel, U. Alkemper, and W. Eberhardt, Ferromagnetic order in ultrathin Rh layers on Fe(100), Phys. Rev. B **46**, 12888 (1992).
[18] E. Hüger and K. Osuch, Ferromagnetism in body centred cubic Rh, Solid State Commun. **131**, 175 (2004).
[19] H. Ohno, Making nonmagnetic semiconductors ferromagnetic, Science **281**, 951 (1998).
[20] M. Friák, M. Šob, and V. Vitek, *Ab initio* calculation of phase boundaries in iron along the bcc-fcc transformation path and magnetism of iron overlayers, Phys. Rev. B **63**, 052405 (2001).
[21] M. Zelený and M. Šob, Theoretical studies of epitaxially grown Co and Ni thin films on (111) metallic substrates, Phys. Rev. B **77**, 155435 (2008).
[22] M. Zelený, D. Legut, and M. Šob, *Ab initio* study of Co and Ni under uniaxial and biaxial loading and in epitaxial overlayers, Phys. Rev. B **78**, 224105 (2008).
[23] M. Zelený, M. Friák, and M. Šob, *Ab initio* study of energetics and magnetism of Fe, Co, and Ni along the trigonal deformation path, Phys. Rev. B **83**, 184424 (2011).
[24] Y. Oba, T. Sato, and T. Shinohara, Ferromagnetism induced by strains in Pd nanoparticles, Phys. Rev. B **78**, 224417 (2008).
[25] S. S. Alexandre, E. Anglada, J. M. Soler, and F. Yndurain, Magnetism of two-dimensional defects in Pd: Stacking faults, twin boundaries, and surfaces, Phys. Rev. B **74**, 054405 (2006).
[26] Y. Sun, J. D. Burton, and E. Y. Tsymbal, Electrically driven magnetism on a Pd thin film, Phys. Rev. B **81**, 064413 (2010).
[27] S. Mirbt, B. Johansson, and H. L. Skriver, Quantum-well-driven magnetism in thin films, Phys. Rev. B **53**, R13310 (1996).
[28] A. M. N. Niklasson, S. Mirbt, H. L. Skriver, and B. Johansson, Quantum-well-induced ferromagnetism in thin films, Phys. Rev. B **56**, 3276 (1997).
[29] S. C. Hong, J. I. Lee, and R. Wu, Ferromagnetism in Pd thin films induced by quantum well states, Phys. Rev. B **75**, 172402 (2007).
[30] S. Sakuragi, T. Sakai, S. Urata, S. Aihara, A. Shinto, H. Kageshima, M. Sawada, H. Namatame, M. Taniguchi, and T. Sato, Thickness-dependent appearance of ferromagnetism in Pd(100) ultrathin films, Phys. Rev. B **90**, 054411 (2014).
[31] R. Félix-Medina, M. Leyva-Lucero, and S. Meza-Aguilar, Magnetism of Ru and Rh thin films on Ag(001) substrate: ab initio calculations, Eur. Phys. J. B **69**, 195 (2009).
[32] R. Wu and A. J. Freeman, Possible 4d ferromagnetism of Rh and Ru overlayers on a Ag(001) substrate, Phys. Rev. B **45**, 7222 (1992).
[33] Y.-R. Jang, S. C. Hong, C. S. Chang, L. H. Cho, and J. I. Lee, A First-principles study of the possible magnetism of Rh in the Cu/Rh/Cu(001) system, J. Korean Phys. Soc. **34**, 450 (1999).
[34] V. Martin, W. Meyer, C. Giovanardi, L. Hammer, K. Heinz, Z. Tian, D. Sander, and J. Kirschner, Pseudomorphic growth of Fe monolayers on Ir(001)-(1×1): From a fct precursor to a bct film, Phys. Rev. B **76**, 205418 (2007).
[35] P. Alippi, P. M. Marcus, and M. Scheffler, Strained Tetragonal States and Bain Paths in Metals, Phys. Rev. Lett. **78**, 3892 (1997).
[36] P. M. Marcus and P. Alippi, Tetragonal states from epitaxial strain on metal films, Phys. Rev. B **57**, 1971 (1998).
[37] S. Schönecker, M. Richter, K. Koepernik, and H. Eschrig, Prediction of first-order martensitic transitions in strained epitaxial films, New J. Phys. **17**, 023005 (2015).
[38] D. Legut, M. Friák, and M. Šob, Why Is Polonium Simple Cubic and So Highly Anisotropic? Phys. Rev. Lett. **99**, 016402 (2007).
[39] D. Legut, M. Friák, and M. Šob, Phase stability, elasticity, and theoretical strength of polonium from first principles, Phys. Rev. B **81**, 214118 (2010).
[40] A. de Siervo, E. De Biasi, F. Garcia, R. Landers, M. D. Martins, and W. A. A. Macedo, Surface structure determination of Pd ultrathin films on Ru(0001): Possible magnetic behavior, Phys. Rev. B **76**, 075432 (2007).
[41] D. A. Stewart, Magnetism in coaxial palladium nanowires, J. Appl. Phys. **101**, 09D503 (2007).
[42] N. Stojić, N. Binggeli, and M. Altarelli, Surface magnetism of Rh(001) from LDA+U calculations, Phys. Rev. B **73**, 100405 (2006).
[43] E. Hüger, T. Káňa, and M. Šob, A mechanism of inhibition of phase transitions in nano-grained close-packed Pd thin films, Calphad **34**, 421 (2010).
[44] P. Blaha, K. Schwarz, G. K. H. Madsen, D. Kvasnicka, and J. Luitz, *WIEN2k, An Augmented Plane Wave Plus Local Orbitals Program for Calculating Crystal Properties* (Vienna University of Technology, Vienna, 2001).
[45] D. M. Ceperley and B. J. Alder, Ground State of the Electron Gas by a Stochastic Method, Phys. Rev. Lett. **45**, 566 (1980).
[46] J. P. Perdew, K. Burke, and M. Ernzerhof, Generalized Gradient Approximation Made Simple, Phys. Rev. Lett. **77**, 3865 (1996).
[47] J. P. Perdew, A. Ruzsinszky, G. I. Csonka, O. A. Vydrov, G. E. Scuseria, L. A. Constantin, X. Zhou, and K. Burke, Restoring the Density-Gradient Expansion for Exchange in Solids and Surfaces, Phys. Rev. Lett. **100**, 136406 (2008).
[48] Z. Wu and R. E. Cohen, More accurate generalized gradient approximation for solids, Phys. Rev. B **73**, 235116 (2006).
[49] J. A. Rayne, Elastic constants of palladium from 4.2–300°K, Phys. Rev. **118**, 1545 (1960).
[50] M. Sigalas, D. A. Papaconstantopoulos, and N. C. Bacalis, Total energy and band structure of the 3d, 4d, and 5d metals, Phys. Rev. B **45**, 5777 (1992).
[51] E. Walker, J. Ashkenazi, and M. Dacorogna, Elastic moduli of rhodium: Correct prediction by a new theoretical method, Phys. Rev. B **24**, 2254 (1981).
[52] A. Eichler, K.-P. Bohnen, W. Reichardt, and J. Hafner, Phonon dispersion relation in rhodium: Ab initio calculations and neutron-scattering investigations, Phys. Rev. B **57**, 324 (1998).
[53] H. J. Monkhorst and J. D. Pack, Special points for Brillouin-zone integrations, Phys. Rev. B **13**, 5188 (1976).
[54] E. E. Fullerton, D. Stoeffler, K. Ounadjela, B. Heinrich, Z. Celinski, and J. A. C. Bland, Structure and magnetism of epitaxially strained Pd(001) films on Fe(001): Experiment and theory, Phys. Rev. B **51**, 6364 (1995).
[55] A. L. N. Pinheiro, M. S. Zei, M. F. Luo, and G. Ertl, The epitaxial growth of Pd electrodeposition on Au(100) studied by LEED and RHEED, Surf. Sci. **600**, 641 (2006).
[56] G. Renaud, A. Barbier, and O. Robach, Growth, structure, and morphology of the Pd/MgO(001) interface: Epitaxial site and interfacial distance, Phys. Rev. B **60**, 5872 (1999).
[57] C. Konvicka, A. Hammerschmid, M. Schmid, and P. Varga, Stabilizing single metal adatoms at room temperature: Pd on C- and O-covered V(100), Surf. Sci. **496**, 209 (2002).

[58] M. F. Carazzolle, S. S. Maluf, A. de Siervo, P. A. P. Nascente, R. Landers, and G. G. Kleiman, Surface composition and structure of palladium ultra-thin films deposited on Ni(111), Surf. Sci. **600**, 2268 (2006).

[59] S. Terada, T. Yokoyama, N. Saito, Y. Okamoto, and T. Ohta, Growth and moiré superstructure of palladium films on Ni(111) studied by STM, Surf. Sci. **433–435**, 657 (1999).

[60] S. S. Chao, E.-A. Knabbe, and R. W. Vook, Auger line shape changes in epitaxial (111)Pd/(111)Cu films, Surf. Sci. **100**, 581 (1980).

[61] R. W. Vook, T. J. Swirbel, and S. S. Chao, Work function changes in the (111)Pd/(111)Cu and CO/(111)Pd/(111)Cu systems, Surf. Sci. **33–34**, 220 (1988).

[62] R. Paniago, A. de Siervo, E. A. Soares, H.-D. Pfannes, and R. Landers, Pd growth on Cu(111): Stress relaxation through surface alloying? Surf. Sci. **560**, 27 (2004).

[63] B. Santos, J. M. Puerta, J. I. Cerda, T. Herranz, K. F. McCarty, and J. de la Figuera, Structure of ultrathin Pd films determined by low-energy electron microscopy and diffraction, New J. Phys. **12**, 023023 (2010).

[64] H. A. Etman, Z. V. Zheleva, G. Held, and R. A. Bennett, Epitaxial growth of ultrathin palladium films on Re{0001}, J. Phys. Chem. C **115**, 4191 (2011).

[65] R. Meyer, M. Bäumer, S. K. Shaikhutdinov, and H.-J. Freund, Two-dimensional growth of Pd on a thin FeO(111) film: A physical manifestation of strong metal-support interaction, Surf. Sci. **546**, L813 (2003).

[66] S. K. Shaikhutdinov, R. Meyer, D. Lahav, M. Bäumer, T. Klüner, and H.-J. Freund, Surface Phase Transitions Induced by Electron Mediated Adatom-Adatom Interaction, Phys. Rev. Lett. **91**, 076102 (2003).

[67] M. J. Ball, C. A. Lucas, N. M. Markovic, V. Stamenkovic, and P. N. Ross, From sub-monolayer to multilayer—an in situ X-ray diffraction study of the growth of Pd films on Pt(111), Surf. Sci. **518**, 201 (2002).

[68] K. Mašek and V. Matolín, RHEED investigation of lattice deformations of α-Al_2O_3 supported Pd particles, Eur. Phys. J. D **9**, 557 (1999).

[69] W. Schlenk and E. Bauer, Properties of ultrathin layers of palladium on a tungsten {110} surface, Surf. Sci. **93**, 9 (1980).

[70] E. Hüger, Epitaxy in the light of the crystal phase transformation: Stabilization of late transition metal and noble metal films in hexagonal and body-centred tetragonal phases by epitaxial growth (unpublished).

[71] Y. He, A. P. Seitsonen, and H. Over, Irregular stacking sequence in the initial growth of ultrathin Rh films on Ru(0001), Phys. Rev. B **72**, 075432 (2005).

[72] G. J. P. Abreu, A. Pancotti, L. H. de Lima, R. Landers, and A. de Siervo, Photoelectron diffraction study of Rh nanoparticles growth on Fe_3O_4/Pd(111) ultrathin film, J. Nanopart. Res. **15**, 1510 (2013).

[73] V. L. Moruzzi and P. M. Marcus, Magnetism in fcc rhodium and palladium, Phys. Rev. B **39**, 471 (1989).

[74] S. Schönecker, M. Richter, K. Koepernik, and H. Eschrig, Ferromagnetic elements by epitaxial growth: A density functional prediction, Phys. Rev. B **85**, 024407 (2012).

[75] N. W. Ashcroft and N. D. Mermin, *Solid State Physics* (Brooks/Cole, Orlando, 1976).

[76] L. Vitos, B. Johansson, and J. Kollár, Size-dependent paramagnetic-ferromagnetic phase transition in palladium clusters, Phys. Rev. B **62**, R11957 (2000).

[77] M. Moseler, H. Häkkinen, R. N. Barnett, and U. Landman, Structure and Magnetism of Neutral and Anionic Palladium Clusters, Phys. Rev. Lett. **86**, 2545 (2001).

[78] B. Sampedro, P. Crespo, A. Hernando, R. Litrán, J. C. S. López, C. L. Cartes, A. Fernandez, J. Ramírez, J. G. Calbet, and M. Vallet, Ferromagnetism in fcc Twinned 2.4 nm Size Pd Nanoparticles, Phys. Rev. Lett. **91**, 237203 (2003).

[79] N. Takano, T. Kai, K. Shiiki, and F. Terasaki, Effect of copious vacancies on magnetims of Pd, Solid State Commun. **97**, 153 (1996).

[80] M. M. Sigalas and D. A. Papaconstantopoulos, Calculations of the total energy, electron-phonon interaction, and Stoner parameter for metals, Phys. Rev. B **50**, 7255 (1994).

[81] I. Tsiaoussis, C. B. Lioutas, and N. Frangis, Structural models for twin interfaces in Pd thin films, J. Microsc. **223**, 208 (2006).

[82] M. Friák, Electronic structure, diffusion-less phase transformations and the stability of phases, Ph.D. thesis, Masaryk University, Brno, Czech Republic, 2002.